Article

Over-Actuated Underwater Robots - Configuration Matrix Design and Perspectives

Tho Dang [1,†,*], Lionel Lapierre [1,†], Rene Zapata [1,†], Benoit Ropars [2,†] and Pascal Lepinay [1,†]

[1] Laboratory of Informatics, Robotics and MicroElectronics (LIRMM) (UMR 5506 CNRS—UM), Université Montpellier, 161 rue Ada, CEDEX 5, 34392 Montpellier, France; danghuu@lirmm.com; lapierre@lirmm.fr; zapata@lirmm.fr; lepinay@lirmm.fr
[2] Reeds company; ropars@lirmm.com
* Correspondence: danghuu@lirmm.com; lapierre@lirmm.fr
† These authors contributed equally to this work.

Abstract: This paper presents the properties and design procedure of configuration matrix of over-actuated marine systems. Performance indices are introduced and analyzed. The problem is formulated as a multi-objective optimization problem. Simulation and experimental results are shown to prove efficiency of the proposed method.

Keywords: Over-actuated underwater robots, Multi-objective optimization, Underwater robots, Performance indices

Citation: T, Dang.; L, Lapierre.; R, Zapata.;B, Ropars.; P, Lepinay. Over-Actuated Underwater Robots - Configuration Matrix Design and Perspectives. Title. *Journal Not Specified* **2021**, *1*, 0. https://doi.org/

Received:
Accepted:
Published:

1. Introduction

Actuation System (AS) is an important part of marine robots. The AS groups the different actuators carried by the system. Following the generic Navigation-Guidance-Control (NGC) control structure, the AS is in charge of realizing the desired force ($\mathbf{F}_B^d$) provided by the control system (see Figure 1). Following Figure 1, the Sensorial Stage

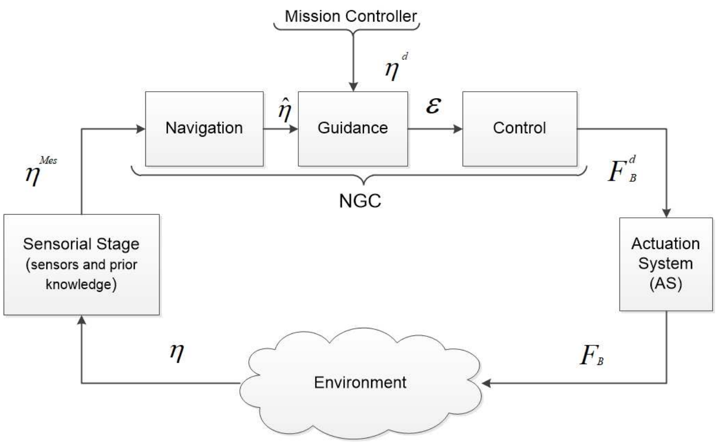

Figure 1. NGC structure augmented with the Actuation System and Sensorial Stage

uses sensors measurement and prior knowledge of the environment to ~~provide the~~ navigation system the necessary information to compute an estimation of system state ($\hat{\eta}$). Then the guidance system uses this estimation and the reference system state (η^d) provided by the mission controller to compute the error function (ε). The control system is then in charge of computing the desired force ($\mathbf{F}_B^d$) in order to reduce the error function to zero. Note that classically this desired force is expressed in the body frame. Afterwards, the *Actuation system* produces on the environment a resulting force ($\mathbf{F}_B$), which should be as close as possible to $\mathbf{F}_B^d$. Note that, in this paper, desired force ($\mathbf{F}_B^d$) and resulting force ($\mathbf{F}_B$) are (6×1) vectors and include force and torque elements.

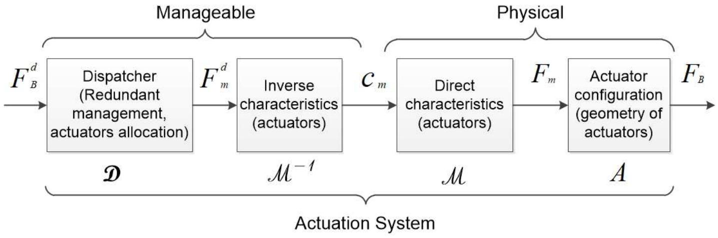

Figure 2. Actuation system scheme

Inside the AS block, referring to Figure 2, the desired force ($\mathbf{F}_B^d$) is the output of the controller. Then the Dispatcher ($\mathcal{D}$) considers actuator allocation method (and eventually ~~redundant~~ management) to compute the desired actuators force ($\mathbf{F}_m^d$) that each actuator has to produce. The inverse actuator characteristics are then considered in order to compute the actuator inputs ($\mathbf{c}_m$). Once applied, $\mathbf{c}_m$ can produce actuator forces ($\mathbf{F}_m$). The resulting force $\mathbf{F}_B$ is produced with respect to the actuator configuration ($\mathbf{A}$). The properties of the AS are indeed dependent of the actuator configuration (position and attitude of actuators with respect to the body frame), actuator dynamics (response characteristics), and dispatcher (control allocation, redundant management) (see Figure 2), and afford the system with different properties. Let's consider in the following that n is the number of Degrees of Freedom (DoFs) of the system, and m is the number of actuators. If the system carries less actuators than DoFs, it is said to be *under-actuated* (in that case, $\mathbf{A}$ will be a $(n \times m)$ matrix where $n > m$). Long-range autonomous underwater vehicles (AUVs) and, for the terrestrial case, unicycle wheeled vehicles belong this category [1]. In that case, specific nonlinear guidance strategies have to be used [2]. If the system carries more actuators than DoFs, it is said to be *redundant* ($n < m$). Then there are different solutions ($\mathbf{c}_m$) to produce an identical resulting force ($\mathbf{F}_B$). Indeed, $\mathcal{D}$ is one of the multiple possible inverses of $\mathbf{A}$, classically, $\mathcal{D} = \mathbf{A}^+$ where $\mathbf{A}^+$ is the Moore-Penrose pseudo-inverse. The properties of the AS plays a pivotal role in the system performances, in terms of achievable dynamics, manoeuvrability, robustness and dependability. The properties of an *over-actuated* system have been studied in aerospace control, where critical safety is required [3], and for marine vehicles [4], where the harsh oceanic condition may easily produce actuator failure. Redundancy has also been used in [5] in order to compensate different and unknown actuator responses. The domain of robotic manipulator has also extensively studied this question of redundancy; especially with recent works on humanoid robotics, where task function approach [6] has been used to achieve concurrently equilibriums [7], walking pattern following [8] and multi-contact management [9].

For a global evaluation of an *Actuation System*, we should of course consider many factors, including redundant management, control allocation method, actuator characteristic (inverse and direct), and actuator configuration. This paper focuses on the study of actuator configuration, other problems can be referred to [5] and references therein.

Different performance criteria related to the actuator configuration design have been proposed. For mobile manipulation, *manipulability index* [10] measures the manipulation capability of the end-effector. Intuitively, this index regards the set of all end-effector velocities which is realizable by joint velocities. This set is called hyper-manipulability ellipsoid. This index is quantified by computing hyper-manipulability ellipsoid properties. Based on these properties, there are different ways to quantify the manipulability index, including the volume of hyper-manipulability ellipsoid, the ratio of the minimum and maximum radii of the hyper-ellipsoid, the minimum radius of the hyper-ellipsoid. The selection depends on the purpose of evaluation. When the uniformity of manipulating ability is important, the ratio of two radii of the hyper-ellipsoid is chosen (optimal value will be closed to 1). Otherwise, the minimum radius of the hyper-ellipsoid is suited for the case where the minimum manipulating ability might be critical [11]. Another criterion, *attainability* ([12], [13], [14]), was studied using workspace volume estimation.

In underwater robotic field, *manipulability index*, *energetic index*, and *force index* were introduced in [15] and manipulability index was applied in [16]. Specifically, the *manipulability index* is used to measure the system ability to exert a desired force ~~at~~ a specific actuator configuration. So, the closer to 1 this index is, better the robot isotropy is, i.e, the robot can exert the same forces/torques in any directions. The *energetic index* is a measurement of the variation of system energy when the direction of desired force changes. This is ~~realized~~ by ~~a measurement of~~ energy consumption when the direction of a~~n~~ ~~unit~~ desired force changes all over a 3D sphere. The basic idea of energetic index is to keep system's energy consumption constant and as low as possible when the direction of action changes. The *force index* is used to measure the ratio between actual maximum and minimum realizing forces. However, these studies only consider a given and fixed actuator configuration. Regarding ~~to~~ the design of actuator configuration of an over-actuated underwater robot, a general problem is: how to achieve an optimal configuration considering different performance indices. This is challenging ~~and~~ raises two specific questions:

1. How to define general and typical indices to evaluate an actuator configuration of an over-actuated underwater robot.
2. How to solve the complex optimal problem, which is normally non-convex and has some conflicting objectives

This paper focuses on the design of the actuator configuration for an over-actuated underwater robot with the contributions outlined below:

1. Propose performance indices to evaluate ~~these of~~ an actuator configuration of underwater robots.
2. Optimize an actuator configuration design of an over-actuated underwater robot with respect to different performance indices simultaneously.

This paper focuses on the design of an actuator configuration of an over-actuated underwater robot which optimizes different performance indices. Mathematically, an actuator configuration is a mapping between an actuator force vector and a resulting force vector (*note that these vectors include force and torque elements*). Since we are considering an underwater robot equipped with thrusters, the mapping will be from a thruster force vector ($\mathbf{F}_m$ space) to a body-frame ~~force~~ vector ($\mathbf{F}_B$ space), (see Figure 3). The mapping is a matrix ~~with some names~~ in the literature such as: control effectiveness matrix [4], [17] static transformation matrix [18], geometrical distribution of thrusters [19], configuration matrix [16]. In this paper, the mapping of an actuator configuration is called a *configuration matrix*, denoted as $\mathbf{A}$.

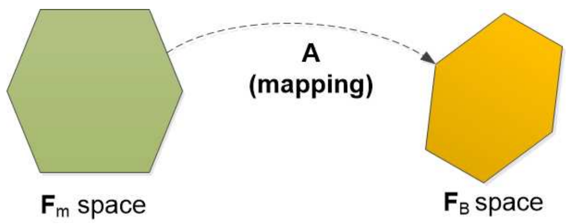

Figure 3. Actuator configuration mapping

The paper is organized as follows. Notations are shown in the section 2. Problem formulation and performance indices are described in the section 3. Problem solution is displayed in the section 4. Simulation results and analyses are depicted in the section 5. Real experiments are depicted in the section 6. Finally, conclusions and future works are discussed in the section 7.

Table 1. Notations

$\mathbf{A}$	Configuration matrix
$\mathbf{A}^+$	Moore-Penrose pseudo-inverse of $\mathbf{A}$ matrix
$\mathbf{u}_i$	(3×1)- unit vector of direction of the i^{th} thruster
$\mathbf{r}_i$	(3×1)- unit vector of position of the i^{th} thruster
$\mathbf{F}_m$	$(m \times 1)$- Force vector of m thrusters
$F_{m,i}$	Force magnitude of the i^{th} thruster
$\mathbf{F}_B^d$	(6×1)- Desired force (force and torque elements) w.r.t body frame
$\mathbf{F}_B = \binom{\mathbf{F}}{\mathbf{\Gamma}}$	(6×1)- Resulting force (force and torque elements) w.r.t body frame
$\mathbf{c}_m$	$(m \times 1)$- Input vector of thrusters
$\otimes$	Cross product
$\lVert \cdot \rVert$	Euclidian norm
$\lVert \cdot \rVert_p$	p-norm
m	the number of thrusters
n	the number of degree of freedoms (DoFs)
$\mathbf{F}$	(3×1)-the vector of force elements in the resulting force $\mathbf{F}_B$
$\mathbf{\Gamma}$	(3×1)-the vector of torque elements in the resulting force $\mathbf{F}_B$

2. Notation

This section depicts most of notations used in the whole paper. However, further notations will be introduced when needed. In order to ~~clear~~ the notations, a given robot configuration is shown in Figure 4 and detail explanations are given in Table 1.

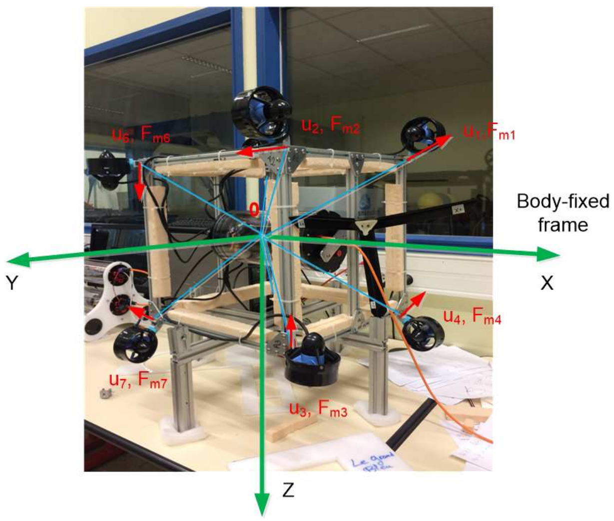

Figure 4. A given robot configuration

3. Problem Formulation

The relation ~~of~~ desired force ($\mathbf{F}_B^d$) and resulting force ($\mathbf{F}_B$) ~~belongs to~~ different ~~factors~~ (see Figure 2). This paper only focuses on actuator configuration. Therefore, three assumptions are ~~outlined below:~~

1. *Inverse characteristics and direct characteristics of actuators are perfectly known, i.e,* $\mathbf{F}_m^d = \mathbf{F}_m$
2. *Dispatcher is the Moore-Penrose pseudo-inverse of actuators configuration, i.e, if actuators configuration is* $\mathbf{A}$ *matrix, dispatcher is* $\boldsymbol{\mathcal{D}} = \mathbf{A}^+$
3. *All actuators have the same characteristics*

3.1. Model of actuator configuration

This part describes how to model an actuator configuration of an over-actuated underwater robot equipped with thrusters. A thruster is modelled by ~~its~~ position and direction with respect to body~~-~~frame of the robot. The position of the i^{th} thruster is described by a~~n~~ unit position vector $\mathbf{r}_i$ and distance d_i to Center of Mass (CM) in the body~~-~~frame. The direction of i^{th} thruster is represented by a~~n~~ unit vector direction $\mathbf{u}_i$ with respect to the body frame as in Figure 5, and the i^{th} thruster ~~propels~~ a force with magnitude ~~of~~ $F_{m,i}$. The relation of thruster force vector and resulting force ~~one~~ (note that this space includes force elements ($\mathbf{F}$) and torque elements ($\mathbf{\Gamma}$)) is described in Equation (1).

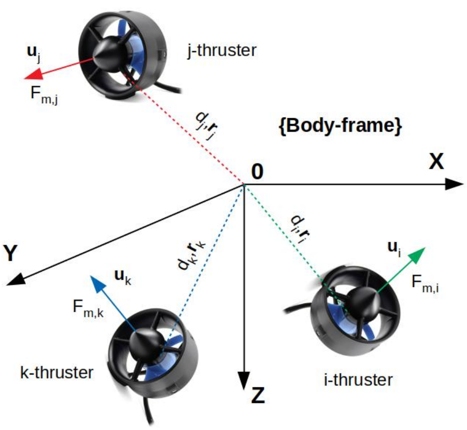

Figure 5. Actuator configuration model

$$\mathbf{F}_B = \mathbf{A}\mathbf{F}_m = \begin{pmatrix} \mathbf{F} \\ \mathbf{\Gamma} \end{pmatrix} \tag{1}$$

where $\mathbf{F}_B = [F_u \quad F_v \quad F_w \quad F_p \quad F_q \quad F_r]^T \in \mathbb{R}^6$, $\mathbf{A} \in \mathbb{R}^{6\times m}$, and $\mathbf{F}_m = [F_{m,1} \quad F_{m,2} \quad ... \quad F_{m,m}]^T \in$ $\mathbb{R}^m$, and m is the number of thrusters, $m > 6$. The configuration matrix $\mathbf{A}$ is described:

$$\begin{aligned} \mathbf{A} &= \begin{pmatrix} \mathbf{u}_1 & \mathbf{u}_2 & \cdots & \mathbf{u}_m \\ d_1\mathbf{r}_1 \otimes \mathbf{u}_1 & d_2\mathbf{r}_2 \otimes \mathbf{u}_2 & \cdots & d_m\mathbf{r}_m \otimes \mathbf{u}_m \end{pmatrix} \\ &= \begin{pmatrix} \mathbf{u}_1 & \mathbf{u}_2 & \cdots & \mathbf{u}_m \\ \boldsymbol{\tau}_1 & \boldsymbol{\tau}_2 & \cdots & \boldsymbol{\tau}_m \end{pmatrix} = \begin{pmatrix} \mathbf{A}_1 \\ \mathbf{A}_2 \end{pmatrix} \end{aligned} \tag{2}$$

where $\mathbf{A}_1$, $\mathbf{A}_2 \in \mathbb{R}^{3\times m}$ are sub-matrices of $\mathbf{A}$ which ~~result~~ force and torque elements respectively. It is obvious to see that $\boldsymbol{\tau}_i^T.\mathbf{u}_i = 0$. This is one ~~of~~ constraint~~s~~ of the configuration matrix.

In this paper, we assume that all distances from thrusters positions to the center of body frame are the same, $d_i = d_j = const, i, j = 1...m,$ ~~$i \neq j$~~. Without loss of generality, we can assume that $d_i = 1, i = 1, ..., m$.

3.2. Manipulability index

As mentioned before, manipulability index was first introduced in [20] for manipulator mechanisms, and there are different ways to quantify the manipulability index. This paper focuses on the isotropy property of a marine robot. Then, the ratio ~~of~~ maximum and minimum radii of the manipulability ellipsoid is chosen (see Figure 6). Because of units consistency, the matrices which ~~results~~ force space, $\mathbf{A}_1$, and torque space, $\mathbf{A}_2$, are investigated separately. However, because of our assumption ~~of~~ d_i, the manipulability index is defined as the condition number of the configuration matrix:

$$I_m = Cond(\mathbf{A}) = \frac{\sigma_{max}}{\sigma_{min}} \tag{3}$$

where σ_{max} and σ_{min} are the maximum and minimum singular value of configuration matrix, $\mathbf{A}$, respectively.

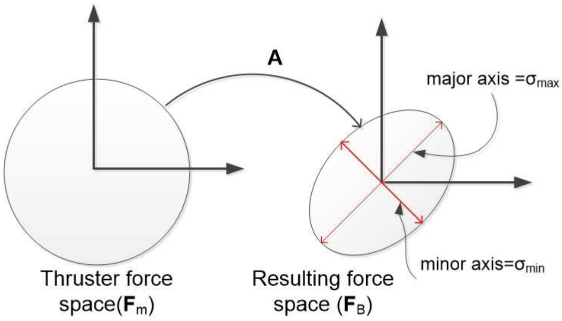

Figure 6. Manipulability ellipsoid with mapping

Following Figure 6, manipulability index investigates the resulting force ellipsoid which is realizable by thruster forces ($\mathbf{F}_m$) such that $\|\mathbf{F}_m\| \leq 1$ (see Theorem in Appendix A). If $I_m = 1$, the robot is isotropic or if $I_m = \infty$, the robot can-not act along at least one direction.

3.3. Energetic index

Energy is very important for marine robots and energy consumption of robots depends on a lot of factors such as mechanical designs, environmental effects, and ~~a~~ specific mission. In order to evaluate the energy performance of an underwater robot, energetic index was introduced in [15]. In this paper, the norm of thruster force vector, $p_E = \|\mathbf{F}_m\|_2$, is used to qualify the energy consumption that an underwater robot uses to produce forces and torques, and can be calculated as ~~in~~ Equation (4).

$$p_E = \|\mathbf{F}_m\|_2 = \sqrt{\sum_{i=1}^{m} F_{mi}^2} = \|\mathbf{A}^+ . \mathbf{F}_B^d\|_2 \tag{4}$$

The energetic index is proposed to measure the variation of energy consumption of an underwater robot when the direction of desired force changes. It is quantified by computing the energy consumption when an unit desired force vector, ($\mathbf{F}_B^d$), changes ~~all~~ over hyper-sphere (see Figure 7 for 3D sphere). Because of units consistency, however, force and torque sphere are computed separately.

For the force sphere case, the unit desired force vector includes an unit vector of force elements and a zero vector of torque elements. For the torque sphere case, the unit desired force vector includes a zero vector of force elements and an unit vector of torque elements. Intuitively, this can be expressed as:

$$\mathbf{F}_B^d = \begin{pmatrix} \mathbf{F} \\ \mathbf{\Gamma} \end{pmatrix} = \begin{cases} \begin{pmatrix} \mathbf{u}_s \\ \mathbf{0} \end{pmatrix}, & \text{for force sphere} \\ \begin{pmatrix} \mathbf{0} \\ \mathbf{u}_s \end{pmatrix}, & \text{for torque sphere.} \end{cases} \tag{5}$$

where $\mathbf{u}_s = [\cos\alpha\cos\beta \quad \sin\alpha\cos\beta \quad \sin\beta]^T$ is a~~n~~ unit vector in spherical coordinates with $\alpha \in [-\pi, \pi]$, and $\beta \in [-\pi/2, \pi/2]$.

According ~~to~~ two cases, the norm of thruster force vector is also divided into two cases as follows:

$$p_E = \begin{cases} p_{Ef} = \|\mathbf{A}^{+}\binom{\mathbf{u}_s}{\mathbf{0}}\|, & \text{for force sphere case} \\ p_{E\Gamma} = \|\mathbf{A}^{+}\binom{\mathbf{0}}{\mathbf{u}_s}\|, & \text{for torque sphere case.} \end{cases} \tag{6}$$

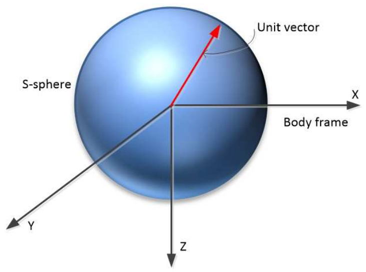

Figure 7. The rotation of unit desired vector in 3D sphere

The energetic index is defined as:

$$I_e = \frac{1}{S}\int_S (w_{ef}p_{Ef} + w_{e\Gamma}p_{E\Gamma})dS \tag{7}$$

where S is the area of 3-dimensional sphere; p_{Ef}, $p_{E\Gamma}$ are the sub-vectors of p_E corresponding ~~with~~ force sphere and torque sphere case, respectively; and w_{ef} and $w_{e\Gamma}$ are weighting coefficients.

3.4. Workspace index

The term of workspace volume was first introduced in [13] for manipulator mechanisms. In this paper, the work space index is used to measure the volume of attainable regions of resulting force space w.r.t body-frame. In general, characteristics of thrusters always have limitations, namely saturations and dead-zones (in this index, dead-zone is ~~neglected).~~ The~~se~~ yield the polytope of thruster force space, $\mathbf{F}_m$ space, denoted as $\mathbb{M}$. By properly choosing configuration matrix, $\mathbf{A} = (\mathbf{A}_1\mathbf{A}_2)^T$, the volume of the resulting force space for force, $\mathbb{F}_F$ space, and the resulting force space for torque, $\mathbb{F}_T$ space can be maximized (see Figure 8). Note that resulting spaces for force and torque are studied separately because of units consistency.

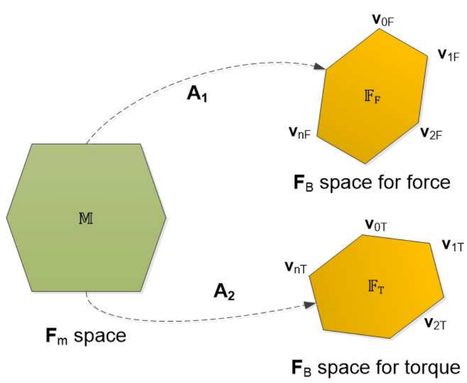

Figure 8. Space Mapping ($\mathbf{v}_i$ is denoted as vertex)

In general, the set $\mathbb{M}$ of thruster forces is known (with given saturations of thrusters), so $\mathbb{M}$ is a polytope and $\mathbb{F}_F$ and $\mathbb{F}_T$ are also polytopes (under ~~a~~ linear transform). We define the workspace index as:

$$I_w = \omega_{wf}Vol(\mathbb{F}_F) + \omega_{w\tau}Vol(\mathbb{F}_T) \tag{8}$$

where Vol is the volume ~~measure of a space~~, ω_{wf} and $\omega_{w\tau}$ are weighting coefficients.

In control perspectives, the larger space's volumes are, the less control efforts are. The design objective is to maximize the workspace index, I_w. Normally, the set $\mathbb{M}$ is convex and its vertices are known. It is easy to find the vertices of $\mathbb{F}_F$ and $\mathbb{F}_T$. Of course $\mathbb{F}_F$ and $\mathbb{F}_T$ are also convex sets (because of linear transformation). This problem becomes a volume computation of convex polytopes.

3.5. Reactive index

Reactive index quantifies how fast the actuation system is able to change the orientation of the resulting force $\mathbf{F}_B$ (ideally $\mathbf{F}_B^d$). Suppose that the robot is traveling in a direction with a set of thruster forces $\mathbf{F}_{m1}$ induced from desired force vector $\mathbf{F}_{B1}^d$. The robot wants to change to another direction (or the same direction with the different manigtude) with the desired force vector $\mathbf{F}_{B2}^d$, so thrusters have to produce another set of thruster forces $\mathbf{F}_{m2}$. The 2-norm of deviation of thruster forces, $\triangle\mathbf{F}_m = \mathbf{F}_{m1} - \mathbf{F}_{m2} = [\triangle F_{m1} \triangle F_{m2} \cdots \triangle F_{mm}]^T$, is considered as the reactive capability of the robot. Referring to the approximation of characteristic of thrusters as Figure 9, the moving time from F_{m1} to F_{m2} is less than the moving time from F_{m1} to F_{m3} (in linear section, the dead-zone of thruster characteristic is neglected in this paper). Hence, we have:

$$\triangle\mathbf{F}_m = \mathbf{A}^+(\mathbf{F}_{B1}^d - \mathbf{F}_{B2}^d) = \mathbf{A}^+\triangle\mathbf{F}_B^d \tag{9}$$

$$\|\triangle\mathbf{F}_m\| = \|\mathbf{A}^+\triangle\mathbf{F}_B^d\| \leq \|\mathbf{A}^+\|\|\triangle\mathbf{F}_B^d\| \tag{10}$$

$$\frac{\|\triangle\mathbf{F}_m\|}{\|\triangle\mathbf{F}_B^d\|} \leq \|\mathbf{A}^+\| \tag{11}$$

From Equation (11), the sensitivity of the thruster forces with respect to desired forces, in other words the variation of thruster forces w.r.t desired forces, is upper-bounded by the norm of pseudo-inverse of the configuration matrix, $\|\mathbf{A}^+\|$. We define the reactive index as:

$$I_{re} = \|\mathbf{A}^+\| \tag{12}$$

It is obvious to see that if this index is ~~more less~~, the robot is more reactive. Then, the objective of design process is to minimize reactive index.

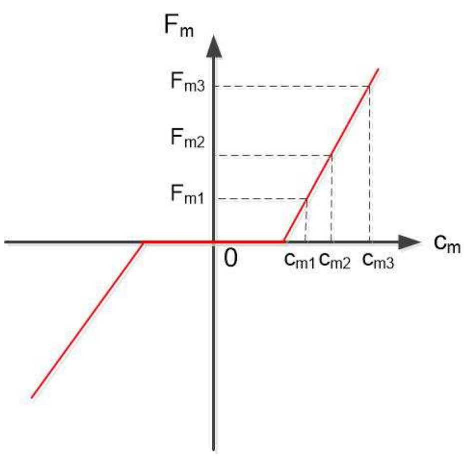

Figure 9. Thruster characteristic approximation

3.6. Robustness index

This criterion measures the robustness level the AS of an underwater robot. It means that if any thrusters of the robot fails, the remaining ones can still perform the robot's mission. In particular, for any $\mathbf{F}_B^d$ vector, there always exists a $\mathbf{F}_m$ vector to satisfy the equation $\mathbf{F}_B = \mathbf{A}\mathbf{F}_m$ and $\mathbf{F}_B$ is as close as possible to $\mathbf{F}_B^d$.

We have:

$$\mathbf{F}_B = \mathbf{A}\mathbf{F}_m = \sum_{i=1}^{m} \mathbf{a}_i F_{m,i} \tag{13}$$

where $\mathbf{a}_i$ is the i^{th} column of the matrix $\mathbf{A}$, and $F_{m,i}$ is the force magnitude of i^{th} thruster.

When one or more thrusters completely fail, the value of $F_{m,i} = 0$. Note that in the case that the i^{th} thruster is partly failed, the value of $F_{m,i}$ remains small (not addressed in this paper). This is equivalent as we consider a corresponding column $\mathbf{a}_i$ of the configuration matrix $\mathbf{A}$ equals to zero vector. Therefore, Equation (13) is equivalent ~~as:~~

$$\mathbf{F}_B = \mathbf{A}^{'}\mathbf{F}_m \tag{14}$$

where $\mathbf{A}^{'}$ matrix is the $\mathbf{A}$ matrix with one or more corresponding columns equal zero vectors.

We discuss hereafter ~~with~~ two questions: conditions of the matrix $\mathbf{A}^{'}$ to guarantee the robustness, and what is the maximum number of failure thrusters?

For addressing two questions, ~~supposing~~ that k-thrusters fail, and Equation (14) is a linear equation system with 6 equations (dimension of $\mathbf{F}_B$ is 6×1) and $(m-k)$ variables because the matrix $\mathbf{A}^{'}$ is $6 \times m$ ~~with~~ k columns are zero vectors. It is obvious to see that if $rank(\mathbf{A}^{'}) = 6$, for given $\mathbf{F}_B^d$, there always exits $\mathbf{F}_m$ such that $\mathbf{F}_B = \mathbf{A}^{'}\mathbf{F}_m$ and $\mathbf{F}_B$ is as close as possible to $\mathbf{F}_B^d$. This can be interpreted that $m - k \geq 6$ or $k \leq m - 6$. The condition ~~of~~ the configuration matrix and the maximum number of failure ~~thrusters~~ that guarantee the robustness of an underwater robot are stated as:

1. *The maximum of failure thrusters: $m - 6$*
2. *Robustness condition: the rank of configuration matrix always equals to 6, i.e, $rank(\mathbf{A}) = 6$, if any columns, from 1 to maximum $(m-6)$, of $\mathbf{A}$ matrix equal to zero vectors. If $rank(\mathbf{A}) < 6$, the system becomes under-actuated, the guidance and control have to change to guarantee the robot's mission. This problem is not addressed in this paper.*

We define the robustness index as:

$$I_{ro} = rank(\mathbf{A}|_{\leq m-6}) = 6 \tag{15}$$

where $\mathbf{A}|_{\leq m-6}$ is the $\mathbf{A}$ matrix ~~with~~ the maximum number of columns being zero is $(m-6)$. This index will be verified in the solving process of the problem.

3.7. Configuration matrix design problem

With all performance indices discussed above, we ~~yield~~ the design problem ~~here:~~

$$\min_{\mathbf{A}} \mathbf{V}(\mathbf{A}) = \min_{\mathbf{A}} [I_m \; I_e \; \frac{1}{I_w} \; I_{re}]^T \qquad s.t \quad \mathbf{A} \in \mathbb{A} \tag{16}$$

where $\mathbf{V}(\mathbf{A})$ is the objective function vector. $\mathbb{A}$ is the feasible set of the configuration matrix $(\mathbf{A})$ including constraints of configuration matrix $(\mathbf{A})$ and robustness index. The reciprocal of the workspace index, $\frac{1}{I_w}$, is in Equation (16) because we want to maximize the workspace index.

This is a multi-objective optimization problem and the unique solution belongs to the convexity of each objective function in the objective vector and the feasible set, $\mathbb{A}$. Note that this optimization problem is with respect to a matrix variable (*matrix optimization*), not a vector variable. However, the optimization techniques for vector variables (*vector optimization*) can be applied here because we do not loose the physical meaning when converting a matrix variable to vector variable in this optimization problem (because of the independent of each column in the matrix derived from the independent ~~of~~ positions and orientations of thrusters).

Specifically, Equation (16) can be rewritten:

$$\begin{aligned} &\min_{\mathbf{A}} \mathbf{V}(\mathbf{A}) = \min_{\mathbf{A}} [I_m \; I_e \; \frac{1}{I_w} \; I_{re}]^T \\ &s.t \quad \|\mathbf{u}_i\| = 1, i = 1, 2, ...m \\ &\qquad \|\boldsymbol{\tau}_i\| \leq 1, i = 1, 2, ...m \\ &\qquad \boldsymbol{\tau}_i^T \mathbf{u}_i = 0, i = 1, 2, ...m \\ &\qquad I_{ro} = rank(\mathbf{A}|_{\leq m-6}) = 6 \end{aligned} \tag{17}$$

The problem (17) is to minimize an objective vector $\mathbf{V}(\mathbf{A})$, including manipulability index, energetic index, reciprocal of workspace index, and reactive index, with respect to configuration matrix, $\mathbf{A}$, satisfies constraints of matrix structure itself and robustness index. It is clear that this is a non-convex and multi-objective optimization problem which normally has many solutions. In the next following sections, we ~~get~~ mathematical analysis and ~~propose~~ a method for multi-objective optimization problem.

4. Problem Solution

Our final objective is to find a distribution (position and orientation) of ~~all~~ thrusters of an underwater robot. This means ~~that you have~~ to get $\mathbf{u}_i$ and $\mathbf{r}_i$ vectors for $i = 1, 2, ..., m$. These vectors can be extracted from configuration matrix $\mathbf{A}$ which is the solution of the problem (17). Recall that our problem (17) is the multi-objective optimization problem with non-convexity, and theoretically, this problem has infinitely many Pareto optimal solutions. Our objective is to find one Pareto optimal solution for building the robot. Analyzing the underlying mathematical properties of the problem helps ~~us~~ to simplify the solving process. Thus, the mathematical analysis of the problem is shown in the next section.

4.1. Mathematical analysis

The configuration matrix $\mathbf{A}$ has the form as:

$$\mathbf{A} = \begin{pmatrix} \mathbf{u}_1 & \mathbf{u}_2 & \cdots & \mathbf{u}_m \\ \boldsymbol{\tau}_1 & \boldsymbol{\tau}_2 & \cdots & \boldsymbol{\tau}_m \end{pmatrix} \tag{18}$$

We have:

$$\mathbf{B} = \mathbf{A}^T\mathbf{A} = \begin{pmatrix} \mathbf{u}_1 & \mathbf{u}_2 & \cdots & \mathbf{u}_m \\ \boldsymbol{\tau}_1 & \boldsymbol{\tau}_2 & \cdots & \boldsymbol{\tau}_m \end{pmatrix}^T \begin{pmatrix} \mathbf{u}_1 & \mathbf{u}_2 & \cdots & \mathbf{u}_m \\ \boldsymbol{\tau}_1 & \boldsymbol{\tau}_2 & \cdots & \boldsymbol{\tau}_m \end{pmatrix} \tag{19}$$

$\mathbf{B}$ is a $m \times m$ symetric matrix where each element is denoted as b_{ij}. We have:

$$\begin{aligned} Tr(\mathbf{B}) &= \sum_{i=1}^{m} b_{ii} \\ &= \sum_{i=1}^{m} \lambda_i \end{aligned} \tag{20}$$

where λ_i is the i^{th} eigenvalue of matrix $\mathbf{B}$.

From Equations (19), and (20), we have:

$$\begin{aligned} \sum_{i=1}^{m} \lambda_i &= \sum_{i=1}^{m} \mathbf{u}_i^T \mathbf{u}_i + \boldsymbol{\tau}_i^T \boldsymbol{\tau}_i \\ &= \sum_{i=1}^{m} \|\mathbf{u}_i\|^2 + \|\boldsymbol{\tau}_i\|^2 \\ \sum_{i=1}^{m} \lambda_i &= \sum_{i=1}^{m} (1 + \|\boldsymbol{\tau}_i\|^2) \end{aligned} \tag{21}$$

In the case of manipulability index optimization, the condition of configuration matrix $\mathbf{A}$ is 1, $cond(\mathbf{A}) = 1$. This means that the maximum singular value equals the minimum singular value, $\sigma_{max} = \sigma_{min}$. Note that the matrix $\mathbf{A}$ is the $n \times m$ matrix with $n < m$. The matrix $\mathbf{A}$ has n non-zero singular values(we have to guarantee that $rank(\mathbf{A}) = n$), then the matrix $\mathbf{B}$ has n non-zero eigenvalues and $m - n$ zero eigenvalues.

In the optimization case of manipulability index, $cond(\mathbf{A}) = 1 \Rightarrow \sigma_{max} = \sigma_{min}$, we have $\lambda_i = \lambda_{max} = \lambda_{min} = \lambda$ ($\sigma = \sqrt{\lambda}$). Equation (21) is rewritten:

$$\begin{aligned} n\lambda &= m + \sum_{i=1}^{m} \|\boldsymbol{\tau}_i\|^2 \\ \lambda &= \frac{m}{n} + \frac{1}{n} \sum_{i=1}^{m} \|\boldsymbol{\tau}_i\|^2 \end{aligned} \tag{22}$$

The fact that $\|\boldsymbol{\tau}_i\|^2 \leq 1$, we have:

$$\lambda \leq 2.\frac{m}{n} \tag{23}$$

Therefore, we have $\lambda_{max} = 2\frac{m}{n}$ when $\|\boldsymbol{\tau}_i\|^2 = 1$.

In the singular value decomposition of a matrix, when $cond(\mathbf{A}) = 1$, the matrix $\mathbf{A}$ can be written as:

$$\mathbf{A} = \mathbf{U}\mathbf{S}\mathbf{V}^T = \mathbf{U}[\sigma]_{n\times m}\mathbf{V}^T \tag{24}$$

where $\mathbf{U} \in \mathbb{R}^{n\times n}$, $\mathbf{V} \in \mathbb{R}^{m\times m}$ are orthogonal matrices, $\mathbf{S} = [\sigma]_{n\times m} = \begin{pmatrix} \sigma & 0 & \cdots & 0 \\ \vdots & \sigma & \cdots & 0 \\ 0 & \cdots & \sigma & 0 \end{pmatrix} \in \mathbb{R}^{n\times m}$

The pseudo-inverse of matrix $\mathbf{A}$ is $\mathbf{A}^+$ can be written:

$$\mathbf{A}^+ = \mathbf{V}\mathbf{S}^+\mathbf{U}^T = \mathbf{V}[\frac{1}{\sigma}]_{m\times n}\mathbf{U}^T \tag{25}$$

Where $\mathbf{S}^+ = [\frac{1}{\sigma}]_{m\times n} = \begin{pmatrix} \frac{1}{\sigma} & \cdots & 0 \\ \vdots & \frac{1}{\sigma} & 0 \\ 0 & 0 & \frac{1}{\sigma} \\ 0 & \cdots & 0 \end{pmatrix} \in \mathbb{R}^{m\times n}$

Our objective with reactive index is to minimize ~~the~~ $\|\mathbf{A}^+\|$. From Equation (25), the reactive index $I_{re} = \|\mathbf{A}^+\| = \frac{1}{\sigma}$, the minimum value of reactive index is equivalent ~~with~~ the maximum value of σ. This leads to the equality of Equation (23) ~~holds.~~

In order to minimize the reactive index and manipulability index, the configuration matrix $\mathbf{A}$ has the structure:

$$\begin{aligned} \mathbf{A} &= \mathbf{USV}^T \\ &= \mathbf{U}\begin{pmatrix} \sigma & 0 & \cdots & 0 & 0 & 0 \\ 0 & \sigma & 0 & \cdots & 0 & 0 \\ 0 & 0 & \sigma & 0 & \cdots & 0 \\ \vdots & \vdots & \vdots & \vdots & \vdots & \vdots \\ 0 & 0 & 0 & \sigma & 0 & 0 \end{pmatrix}\mathbf{V}^T \end{aligned} \tag{26}$$

where $\mathbf{S}(n\times m)$ is like-diagonal and $\sigma = \sqrt{\lambda} = \sqrt{2\frac{m}{n}}$; $\mathbf{U}(n\times n)$ and $\mathbf{V}(m\times m)$ are orthogonal matrices ($\mathbf{UU}^T = \mathbf{I}, \mathbf{VV}^T = \mathbf{I}$). This results can be used as initial value of numerical optimization process and useful for solving the problem.

We continue discussing about the energetic index. First, we introduce a proposition as follows:

Proposition 1. *Let* $\mathbf{M}$ *be a* $p\times q$ *matrix* ($p \geq q$), $\mathbf{M} \in \mathbb{R}^{p\times q}$. *For all* $\mathbf{x} \in \mathbb{R}^q$, *if* $\mathbf{M} = \mathbf{P\Sigma Q}^T$, *where* $\mathbf{P} \in \mathbb{R}^{p\times p}, \mathbf{Q} \in \mathbb{R}^{q\times q}$ *are orthogonal matrices,* $\mathbf{\Sigma} = \begin{pmatrix} \mu & 0 & \cdots & 0 \\ 0 & \mu & \cdots & 0 \\ 0 & \cdots & \mu & 0 \\ 0 & \cdots & 0 & \mu \\ \vdots & \vdots & \vdots & \vdots \\ 0 & 0 & 0 & 0 \end{pmatrix} \in \mathbb{R}^{p\times q}$ *then* $\|\mathbf{Mx}\| = \|\mathbf{M}\|\|\mathbf{x}\|$.

Proof. We have:

$$\|\mathbf{Mx}\|^2 = (\mathbf{Mx})^T(\mathbf{Mx}) = \mathbf{x}^T\mathbf{M}^T\mathbf{Mx} \tag{27}$$

With $\mathbf{M} = \mathbf{P\Sigma Q}^T$

$$\begin{aligned} \|\mathbf{Mx}\|^2 &= \mathbf{x}^T(\mathbf{P\Sigma Q}^T)^T(\mathbf{P\Sigma Q}^T)\mathbf{x} \\ &= \mathbf{x}^T\mathbf{Q\Sigma}^T\mathbf{P}^T\mathbf{P\Sigma Q}^T\mathbf{x} \\ &= \mathbf{x}^T\mathbf{Q\Sigma}^T\mathbf{\Sigma Q}^T\mathbf{x} \end{aligned} \tag{28}$$

We have:

$$
\begin{aligned}
\mathbf{\Sigma}^T\mathbf{\Sigma} &= \begin{pmatrix} \mu & 0 & \cdots & 0 \\ 0 & \mu & \cdots & 0 \\ 0 & \cdots & \mu & 0 \\ 0 & \cdots & 0 & \mu \\ \vdots & \vdots & \vdots & \vdots \\ 0 & 0 & 0 & 0 \end{pmatrix}^T \begin{pmatrix} \mu & 0 & \cdots & 0 \\ 0 & \mu & \cdots & 0 \\ 0 & \cdots & \mu & 0 \\ 0 & \cdots & 0 & \mu \\ \vdots & \vdots & \vdots & \vdots \\ 0 & 0 & 0 & 0 \end{pmatrix} \\
&= \begin{pmatrix} \mu^2 & 0 & \cdots & 0 \\ 0 & \mu^2 & \cdots & 0 \\ \vdots & \vdots & \vdots & \vdots \\ 0 & \cdots & 0 & \mu^2 \end{pmatrix} = \mu^2\mathbf{I}
\end{aligned} \tag{29}
$$

where $\mathbf{I}$ is $q \times q$ identity matrix.

Replacing Equation (29) to (28), we have:

$$
\begin{aligned}
\|\mathbf{Mx}\|^2 &= \mathbf{x}^T\mathbf{V}\mu^2\mathbf{I}\mathbf{V}^T\mathbf{x} \\
&= \mu^2\mathbf{x}^T\mathbf{x} = \|\mathbf{M}\|^2\|\mathbf{x}\|^2
\end{aligned} \tag{30}
$$

Therefore, $\|\mathbf{Mx}\| = \|\mathbf{M}\|\|\mathbf{x}\|$. $\square$

The energetic index is stated as:

$$
I_e = \frac{1}{S}\int_S (w_{ef}\|\mathbf{A}^+(\mathbf{F}_B^d(f)\| + w_{e\Gamma}\|\mathbf{A}^+\mathbf{F}_B^d(\Gamma)\|)dS \tag{31}
$$

~~Choose~~ $w_{ef} = w_{e\Gamma} = 1$ (because desired force vectors, $\mathbf{F}_B^d(f), \mathbf{F}_B^d(\tau)$, are unit), we have:

$$
I_e = \frac{1}{S}\int_S (\|\mathbf{A}^+\mathbf{F}_B^d(f)\| + \|\mathbf{A}^+\mathbf{F}_B^d(\Gamma)\|)dS \tag{32}
$$

In case ~~the minimum of~~ reactive index and manipulability index, the configuration matrix $\mathbf{A}(n \times m)$ has the form as the equation (26), therefore the pseudo-inverse matrix $\mathbf{A}^+(m \times n, \quad m > n)$ has the structure ~~as:~~

$$
\mathbf{A}^+ = \mathbf{V}\mathbf{S}^+\mathbf{U}^T = \mathbf{V}\begin{pmatrix} \frac{1}{\sigma} & 0 & \cdots & 0 \\ 0 & \frac{1}{\sigma} & \cdots & 0 \\ 0 & \cdots & \frac{1}{\sigma} & 0 \\ 0 & \cdots & 0 & \frac{1}{\sigma} \\ \vdots & \vdots & \vdots & \vdots \\ 0 & 0 & 0 & 0 \end{pmatrix}\mathbf{U}^T \tag{33}
$$

where $\mathbf{V}, \mathbf{U}$ are orthogonal matrices.

It is clear that matrix $\mathbf{A}^+$ satisf~~y~~ the condition of Proposition 1. Applying this proposition, we have: $\|\mathbf{A}^+\mathbf{F}_B^d(f)\| = \|\mathbf{A}^+\|\|\mathbf{F}_B^d(f)\|$ and $\|\mathbf{A}^+\mathbf{F}_B^d(\Gamma)\| = \|\mathbf{A}^+\|\|\mathbf{F}_B^d(\Gamma)\|$. Therefore, Equation (32) becomes:

$$I_e = \frac{1}{S}\int_S (\|\mathbf{A}^+\|\|\mathbf{F}_B^d(f)\| + \|\mathbf{A}^+\|\|\mathbf{F}_B^d(\Gamma)\|)dS$$
$$= \frac{1}{S}\|\mathbf{A}^+\|\int_S (\|\mathbf{F}_B^d(f)\| + \|\mathbf{F}_B^d(\Gamma)\|)dS$$
$$= 2\|\mathbf{A}^+\| \tag{34}$$

~~For~~ aforementioned mathematical analysis of the energetic index, we can see that the energetic index belongs to the norm of pseudo-inverse of configuration matrix, $I_{re} = 2\|\mathbf{A}^+\|$, when the configuration matrix $\mathbf{A}$ has the form of (26).

We discuss about the upper-bound of workspace index. For units consistency, the workspace index for force space and for torque space are investigate separately, denoted as I_{wf} and $I_{w\tau}$ respectively. Recall that the objective of workspace index is to maximize the volume of resulting force space ($\mathbf{F}_B$ space) including resulting space for force and resulting space for torque with given ~~the~~ thrusters force ~~space~~ ($\mathbf{F}_m$ space).

The fact that for all vector $\mathbf{F}_m \in \mathbb{R}^m$, $\|\mathbf{A}\mathbf{F}_m\| \leq \|\mathbf{A}\|\|\mathbf{F}_m\|$. The volume of the resulting force space is maximum when the equality holds.

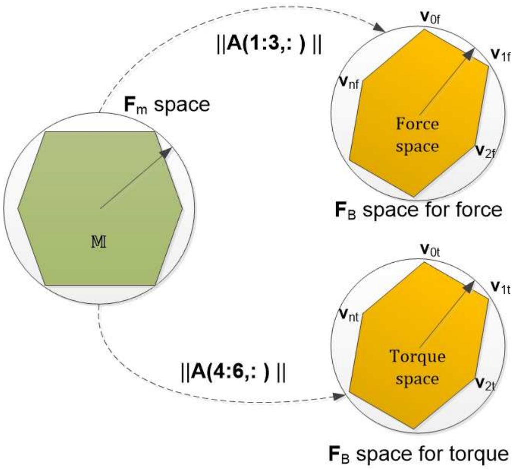

Figure 10. Upper-bound of resulting force space

Following Figure 10, the volume of resulting force spaces ($\mathbf{F}_B$)(force and torque spaces) are always less than the volume of exterior hyper-sphere of $\mathbf{F}_B$ spaces of fore and torque (may be the circumscribed spheres or not). This means that:

$$I_{wF} \leq Vol\cancel{ume}(\mathbf{B}(R1))$$
$$I_{wT} \leq Vol\cancel{ume}(\mathbf{B}(R2)) \tag{35}$$

where $\mathbf{B}(R1)$ and $\mathbf{B}(R2)$ are ~~an~~ Euclidean balls of radius $R1 = \|\mathbf{A}(\mathbf{1}:\mathbf{3},:)\|\|\mathbf{F}_m\| = \|\mathbf{A}_1\|\|\mathbf{F}_m\|$ and of radius $R2 = \|\mathbf{A}(\mathbf{4}:\mathbf{6},:)\|\|\mathbf{F}_m\| = \|\mathbf{A}_2\|\|\mathbf{F}_m\|$ respectively; $\mathbf{A}(\mathbf{1}:\mathbf{3},:)$ is ~~the **A** matrix with three first rows~~, and $\mathbf{A}(\mathbf{4}:\mathbf{6},:)$ ~~is the **A** matrix with three last rows~~.

~~The fact that n-dimensional~~ volume of an Euclidean ball of radius R in n-dimensional Euclidean space is [21]:

$$V_n(R) = \begin{cases} \frac{\pi^k}{k!}R^{2k}, & \text{if } n = 2k \\ \frac{2^{k+1}\pi^k}{(2k+1)!!}R^{2k+1}, & \text{if } n = 2k+1. \end{cases} \tag{36}$$

where $(2k+1)!! = 1.3.5...(2k-1).(2k+1)$.

Proposition 2. *If the configuration matrix* $\mathbf{A}$ *has the form of* (26) *then* $cond(\mathbf{A}_1) = cond(\mathbf{A}_2) = 1$ *and* $\|\mathbf{A}_1\| = \|\mathbf{A}_2\| = \sigma$

Proof. We have:

$$\begin{aligned}\mathbf{A}\mathbf{A}^T &= (\mathbf{USV}^T)(\mathbf{USV}^T)^T = \mathbf{USV}^T\mathbf{VS}^T\mathbf{U}^T \\ &= \mathbf{USS}^T\mathbf{U}^T = \sigma^2\mathbf{I}\end{aligned} \tag{37}$$

On the other hand:

$$\begin{aligned}\mathbf{A}\mathbf{A}^T &= \begin{pmatrix}\mathbf{A}_1 \\ \mathbf{A}_2\end{pmatrix}\begin{pmatrix}\mathbf{A}_1 \\ \mathbf{A}_2\end{pmatrix}^T = \begin{pmatrix}\mathbf{A}_1 \\ \mathbf{A}_2\end{pmatrix}(\mathbf{A}_1^T\mathbf{A}_2^T) \\ &= \begin{pmatrix}\mathbf{A}_1\mathbf{A}_1^T & \mathbf{0} \\ \mathbf{0} & \mathbf{A}_2\mathbf{A}_2^T\end{pmatrix}\end{aligned} \tag{38}$$

From (37) and (38), we have:

$$\begin{aligned}\mathbf{A}_1\mathbf{A}_1^T &= \sigma^2\mathbf{I}_1 \\ \mathbf{A}_2\mathbf{A}_2^T &= \sigma^2\mathbf{I}_2\end{aligned} \tag{39}$$

where $\mathbf{I}_1$ and $\mathbf{I}_2$ are partitioned matrices of matrix $\mathbf{I}$.

From (39) and the uniqueness of singular value decomposition [22], it is obvious to get the structures of $\mathbf{A}_1$ and $\mathbf{A}_2$ are the same as (26) with different dimensions. Therefore, $cond(\mathbf{A}_1) = cond(\mathbf{A}_1) = 1$ and $\|\mathbf{A}_1\| = \|\mathbf{A}_2\| = \sigma$. □

From (35) and (36) and Proposition 2, it is obvious to get the upper-bound of resulting spaces of force and torque of the system, and then the upper-bound of workspace index. Normally, the weighting coefficients in workspace index are chosen ~~as~~ 1 because of our assumption of d_i.

4.2. Problem solution

Based on the above mathematical analys~~es~~, goal attainment method is chosen to solve the problem with given desired values. The idea of this method is to minimize the deviation of desired values and getting values. One advantage of goal attainment method is that the problem do not need to normalize to dimensionless problem. The solution of this method is proven to be ~~Parteo~~ optimal. This method is also suitable when the feasible objective set is non-convex [23]. All Pareto optimal solutions can be found by changing the attainment vector.

Our problem using goal attainment approach becomes:

$$\begin{aligned}&\min_{\mathbf{A},\gamma} \gamma \\ &s.t \quad \mathbf{A} \in \bar{\mathbb{A}} \\ &\qquad\;\; \mathbf{V}(\mathbf{A}) - \mathbf{w}\gamma \leq \mathbf{V}_{goal}\end{aligned} \tag{40}$$

where $\bar{\mathbb{A}} = \mathbb{A} \setminus I_{ro}$, i.e, $\mathbf{A}$ set without robustness index I_{ro}, γ is a slack vector variable, $\mathbf{V}_{goal} = [I_m^d \quad I_e^d \quad \frac{1}{I_w^d} \quad I_{re}^d]$ is the desired objective vector, $\mathbf{w}$ is a attainment vector which can be chosen. The goal attainment method with two objective functions is illustrated in Figure 11. By altering $\mathbf{w}$ vector, we ~~get~~ Pareto optimal solutions. ~~The chosen solution belongs how to choose this attainment vector.~~

Therefore, our solving process includes two phases:

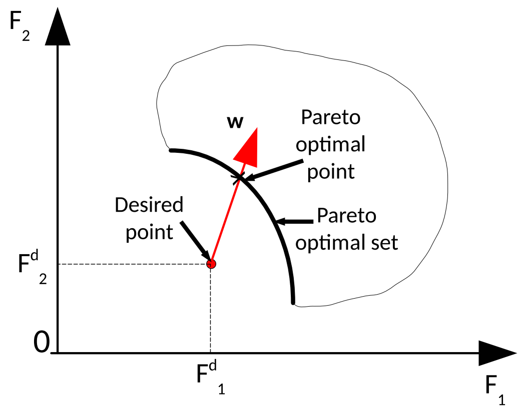

Figure 11. Goal attainment method with two objective functions

1. Phase 1: Find one Pareto solution of configuration matrix with goal attainment method.
2. Phase 2: Check robustness index of the chosen solution in phase 1.

The optimization toolbox in Matlab environment is used to solve our problem.

5. Simulation results

We have designed an over-actuated underwater robot with $m = 8$ thrusters and $n = 6$ degrees of freedom. Two cases are simulated: general case and given position case. In general case, we have to identify both the positions and orientations of 8 thrusters optimizing the performance indices. In given position case, the thrusters are installed at the corners of a cube, we only have to determine the directions of thrusters. In this simulation, thruster characteristic is chosen as in [5], then the maximum and minimum values of thrusters forces are as $F_{imax} = 1.1N$ and $F_{imin} = -0.4N$ respectively. The desired values of performance indices are subsequently $I_m^d = 1, I_e^d = 1.2248, I_{wF}^d = 597.7, I_{wT}^d = 597.7, I_{re}^d = 0.6124$ ($\sigma^{max} = \sqrt{2\frac{m}{n}} = 1.6330$, see Table 2 for more details).

Table 2. Desired values of indices

Index	Optimal formula and condition	Desired Value
I_m^d	$\sigma_{max} = \sigma_{min}$	1
I_e^d	$2\,\lVert\mathbf{A}^+\rVert$	1.2248
$\frac{1}{I_w^d}$	see Equation 35 and 36 and $\frac{1}{I_w^d} = \frac{1}{I_{wF}^d} + \frac{1}{I_{wT}^d}$	0.0033
I_{re}^d	$\frac{1}{\sigma^{max}}$	0.6124

5.1. General case

In this case, the robot is called Ball robot and the positions and orientations of thrusters are not known. The problem (40) is solved as follows:

5.1.1. Phase 1

Optimization toolbox is used to solve the problem (40) with desired goal vector and constraints are as $\mathbf{V}_{goal} = [I_m^d \quad I_e^d \quad \frac{1}{I_w^d} \quad I_{re}^d] = [1 \quad 1.2248 \quad 0.0033 \quad 0.6124]^T$, the constraint set $\bar{\mathbb{A}} = \{\mathbf{A} \in \mathbb{R}^{6\times 8} / \lVert\mathbf{u}_i\rVert = 1, \lVert\boldsymbol{\tau}_i\rVert \leq 1, \boldsymbol{\tau}_i^T\mathbf{u_i} = 0\}$, the attainment vector $\mathbf{w} = [0 \quad 0 \quad 0 \quad 0.0036]^T$.

The simulation results are shown in Figures 12, 13, and 14. The configuration matrix $\mathbf{A}$ and optimal values are shown in Table 3. Specifically, in Figure 12, the positions of thrusters are at the top of blue line, the orientations of thrusters are shown as the red arrow. Furthermore, we can see that the isotropy property of robot is guaranteed (see Figures 13, 14) with sphere shapes of attainable spaces of forces and torques. From Table 3, the getting values of manipulability index, energetic index, and reactive index are almost the same desired values. However, the getting value of workspace index is under-attainment of desired value with an attainment factor.

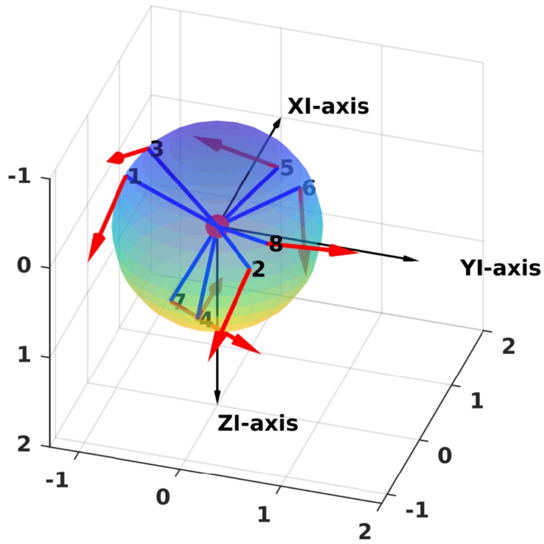

Figure 12. Positions and directions of thrusters (general case)

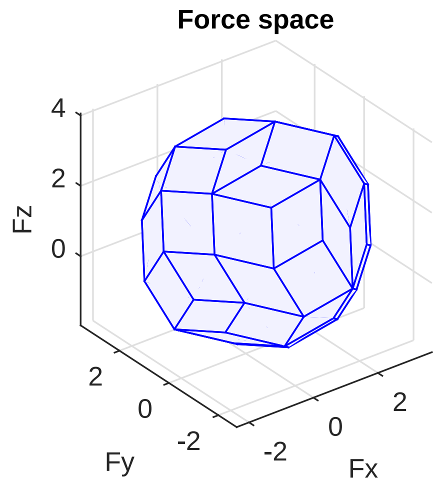

Figure 13. Attainable force space (general case)

5.1.2. Phase 2

In this phase, the robustness index is checked. The optimal configuration matrix **A** in Table 3 satisfies the robustness constraint. Specifically, the maximum number of thrusters that are ~~able to be failed~~ is two.

5.2. Given position case

In this case, the robot is called Cube robot and the positions of thrusters are ~~given~~ at corners of the cube. We just only have to find their orientations. The number of variables in the problem (40) is reduced. The desired objective vector and attainment vector are the same as in general case. The results are presented in the sequel.

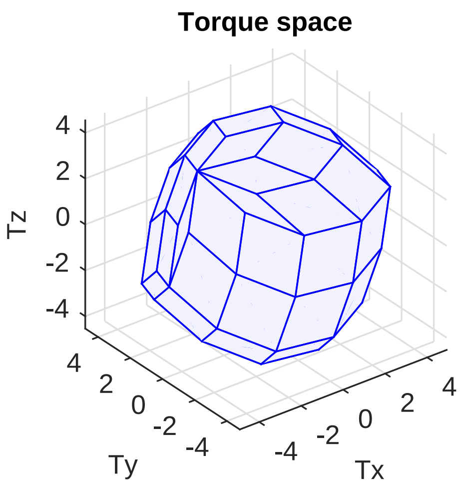

Figure 14. Attainable torque space (general case)

Table 3. Configuration matrix in general case

Configuration matrix	Optimal value	Attainment factor
$\mathbf{A} = \begin{pmatrix} -0.8891 & -0.3645 & 0.5438 & 0.9879 & 0.3134 & 0.0148 & 0.0495 & 0.6090 \\ -0.0985 & -0.3036 & -0.5911 & -0.0608 & -0.9493 & 0.0515 & 0.8919 & 0.7158 \\ 0.4471 & 0.8803 & 0.5957 & 0.1429 & 0.0260 & 0.9986 & 0.4495 & 0.3417 \\ -0.4308 & 0.4701 & -0.8386 & 0.0379 & -0.1336 & 0.5628 & -0.9972 & 0.4758 \\ 0.5107 & 0.7561 & -0.4103 & 0.9868 & -0.0712 & -0.8259 & 0.0690 & 0.0149 \\ -0.7441 & 0.4554 & 0.3583 & 0.1577 & -0.9885 & 0.0342 & -0.0272 & -0.8794 \end{pmatrix}$	$Fval = \begin{pmatrix} 1.0000 \\ 1.2200 \\ 0.0050 \\ 0.6124 \end{pmatrix}$	0.3896

5.2.1. Phase 1

Optimization toolbox is used to solve our problem and simulation results are shown in Figures 15, 16, 17, and Table 4. The directions of thrusters are depicted as red arrows in Figure 15. Similar to the general case, the isotropy property is also guaranteed in this case (see Figure 16 and Figure 17). One Pareto optimal configuration matrix is shown in Table 4. We can see that the getting objective values in Table 4 is the same ~~with in~~ the general case.

5.2.2. Phase 2

The optimal configuration matrix $\mathbf{A}$ in Table 4 satisfies the conditions of robustness index. Similarly, the maximum number of thrusters that can ~~be able to be failed~~ is two.

5.3. A comparison of two configurations

In this section, a comparison of two configurations is illustrated. The choice of configurations is corresponding with a real robot (Cube robot) which is used in experiments in the next section. The first one is a normal configuration (denoted as $\mathbf{C}^1$) ~~in which~~ the thrusters are distributed vertically or horizontally(in practice, this configuration is easier to install as Figure 24). The configuration matrix of $\mathbf{C}^1$ configuration, denoted $\mathbf{A}_1$, is shown in Equation (41).

$$\mathbf{A}_1 = \begin{pmatrix} 0 & 1 & 0 & 0 & 0 & 0 & -1 & 0 \\ 1 & 0 & 0 & -1 & 1 & 0 & 0 & 0 \\ 0 & 0 & -1 & 0 & 0 & 1 & 0 & -1 \\ 0.27 & 0 & -0.27 & 0.27 & 0.27 & 0.27 & 0 & 0.27 \\ 0 & -0.27 & 0.27 & 0 & 0 & 0.27 & -0.27 & -0.27 \\ 0.27 & -0.27 & 0 & 0.27 & 0.27 & 0 & 0.27 & 0 \end{pmatrix} \quad (41)$$

Table 4. Configuration matrix in given position case

Configuration matrix	Optimal value	Attainment factor
$\mathbf{A} = \begin{pmatrix} 0.0836 & 0.6616 & -0.8122 & 0.4785 & -0.6616 & -0.0836 & -0.4785 & -0.8122 \\ 0.7452 & 0.7452 & 0.3337 & 0.3337 & 0.7452 & 0.7452 & 0.3337 & -0.3337 \\ 0.6616 & -0.0836 & -0.4785 & -0.8122 & 0.0836 & -0.6616 & 0.8122 & -0.4785 \\ -0.8122 & 0.4785 & -0.0836 & -0.6616 & -0.4785 & 0.8122 & 0.6616 & -0.0836 \\ -0.3337 & -0.3337 & 0.7452 & 0.7452 & -0.3337 & -0.3337 & 0.7452 & -0.7452 \\ 0.4785 & 0.8122 & 0.6616 & -0.0836 & -0.8122 & -0.4785 & 0.0836 & 0.6616 \end{pmatrix}$	$Fval = \begin{pmatrix} 1.0000 \\ 1.2200 \\ 0.0050 \\ 0.6124 \end{pmatrix}$	0.3868

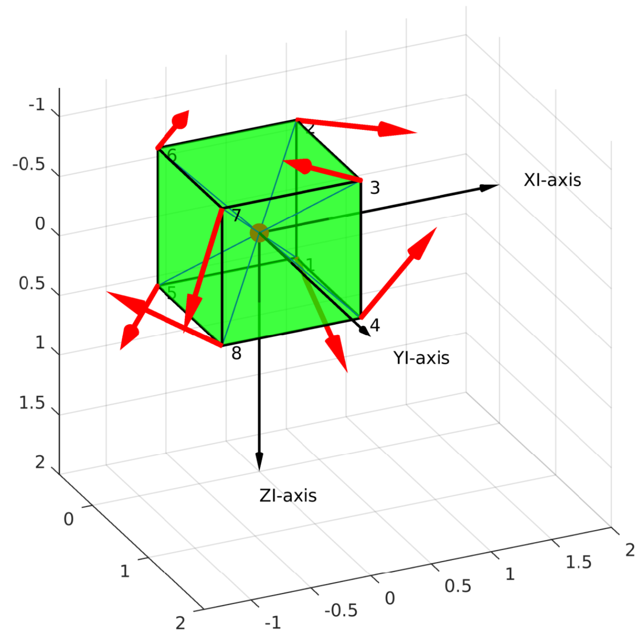

Figure 15. Robot design with directions of thrusters (given position case)

The second one (denoted as $\mathbf{C}^2$) is an optimal configuration, denoted as $\mathbf{A}_2$, which is a solution of optimization problem (given position case) thanks to thruster characteristics of BlueRobotics (Figure 18) and the optimal configuration matrix is shown in Equation (42).

$$\mathbf{A}_2 = \begin{pmatrix} 0.6616 & -0.8122 & 0.4785 & 0.0836 & -0.0836 & -0.4785 & -0.8122 & -0.6616 \\ 0.7452 & 0.3337 & 0.3337 & 0.7452 & 0.7452 & 0.3337 & -0.3337 & 0.7452 \\ -0.0836 & -0.4785 & -0.8122 & 0.6616 & -0.6616 & 0.8122 & -0.4785 & 0.0836 \\ 0.1608 & 0.0111 & -0.2459 & -0.3708 & 0.3642 & 0.2015 & 0.0011 & -0.1658 \\ -0.0989 & 0.3556 & 0.3633 & -0.0989 & -0.1056 & 0.3508 & -0.3456 & -0.1056 \\ 0.3906 & 0.2292 & 0.0044 & 0.1583 & -0.1649 & -0.0254 & 0.2392 & -0.3708 \end{pmatrix} \tag{42}$$

Note that the configuration matrices $\mathbf{A}_1$ and $\mathbf{A}_2$ are calibrated with corresponding geometrical properties of real cube robot in LIRMM Institute, Montpellier University. The attainable force space and torque space corresponding with two configurations $\mathbf{C}^1$ and $\mathbf{C}^2$ are illustrated in Figure 19a and Figure 19b. It is obvious to see that the $\mathbf{C}^2$ configuration is more isotropic than the $\mathbf{C}^1$ configuration. However, for some specific points of attainable fore and torque spaces, the $\mathbf{C}^1$ configuration is ~~greater~~ than the $\mathbf{C}^2$ configuration.

Thanks to the properties of matrices $\mathbf{A}_1$ and $\mathbf{A}_2$ (Equation (41) and (42)) and the thruster characteristic (Figure 18), Table 5 shows the values of performance indices for ~~two~~ configurations. The performances of $\mathbf{C}^2$ configuration are better than ~~ones of~~ $\mathbf{C}^1$. Because of the calibration (the distance d_i is different between motors), the manipulability index (I_m) is larger than 1.

In order to verify the attainability of two configurations (workspace index), incremental torques are applied about ~~X~~, ~~Y~~, and ~~Z~~ axis respectively (Figures 20a, 21a, and 22a), the corresponding PWM (Pulse Width Modulation) inputs ($\mathbf{c}_m$) of 8 thrusters are computed. The results are shown in Figures 20b, 20c, 21b, 21c, 22b, and 22c in which the two PWM's saturation values of thrusters (upper saturation value: 1900, lower saturation value: 1100) are plotted with two bold lines. We can see that the performances of the robot with two configurations are almost the same ~~with~~ the rotation about X and Y axis. However, the $\mathbf{C}^2$ configuration shows better performance ~~with~~ the rotation about Z-axis.

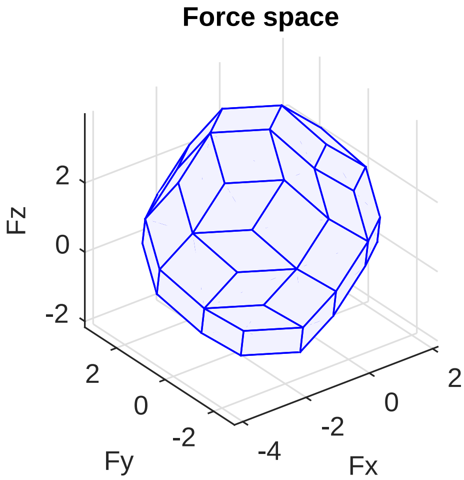

Figure 16. Attainable force space(given position case)

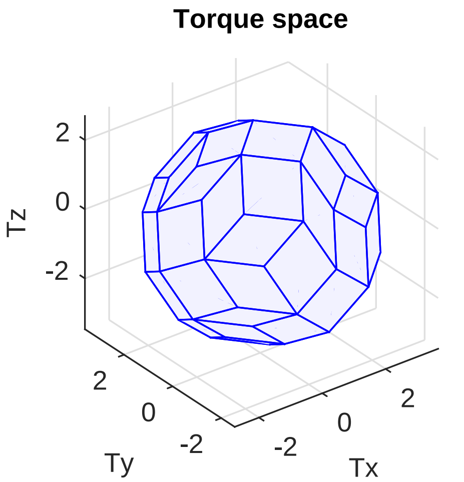

Figure 17. Attainable torque space (given position case)

In fact, the thrusters with $\mathbf{C}^1$ configuration reach saturations very earlier in comparison with the thrusters with $\mathbf{C}^2$ configuration (Figures 22b and 22c).

In order to validate the robustness of the optimal configuration ($\mathbf{C}^2$) in comparison with the normal configuration ($\mathbf{C}^1$), the rank of matrices $\mathbf{A}_1$ and $\mathbf{A}_2$ is checked when arbitrary one or two columns have been nullified. When the resulting matrices are rank deficient, this means that the robustness is not guaranteed because one ~~DoF~~ is not actuated. Therefore, we can not control all 6 DoFs independently. The robustness index in Table 5 shows the checking results. In particular, when the 5^{th} thruster of $\mathbf{C}^1$ configuration fails, the robustness is not guaranteed.

Table 5. Comparison between two configurations(I_{ro} shows the maximum number of thrusters which can be failed to make sure that $rank(\mathbf{A} = 6)$)

No.	Indices	$\mathbf{C}^1$	$\mathbf{C}^2$
1	I_m	7.12	2.559
2	I_e	3.32	2.09
3	I_w	6511536.45	10919428.13
4	I_{re}	4.05	1.56
5	I_{ro}	0	2

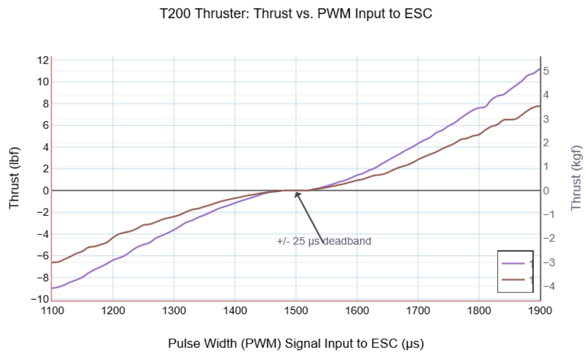

Figure 18. Thruster characteristic(BlueRobotics) [24]

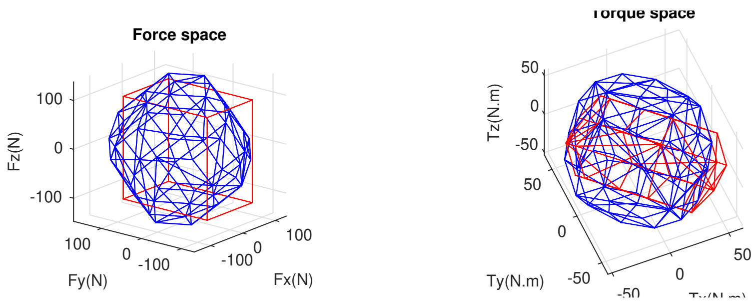

(a) $\mathbf{C}^1$(red), $\mathbf{C}^2$(blue) **(b)** $\mathbf{C}^1$(red), $\mathbf{C}^2$(blue)

Figure 19. Attainable spaces for different configurations

6. Experimental results

Experiments are carried out on Cube robot to compare between two configurations, $\mathbf{C}^1$ (see Figure 24), $\mathbf{C}^2$ (see Figure 25), ~~thanks~~ to swimming pool at Montpellier University (see Figure 26). The Cube in water and a video link for Cube's operations can be seen in Figure 23.

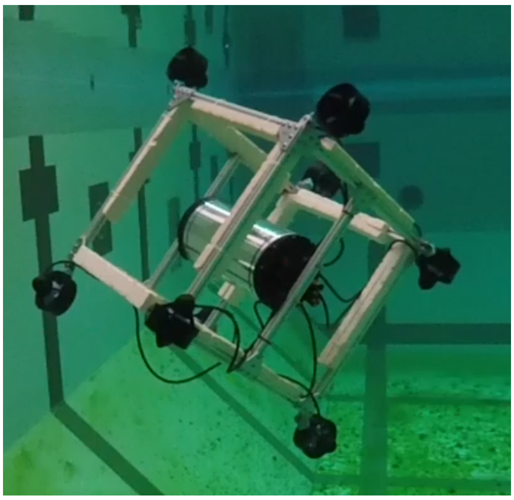

Figure 23. Cubet robot in water https://www.youtube.com/watch?v=RKiWUOxDKdw

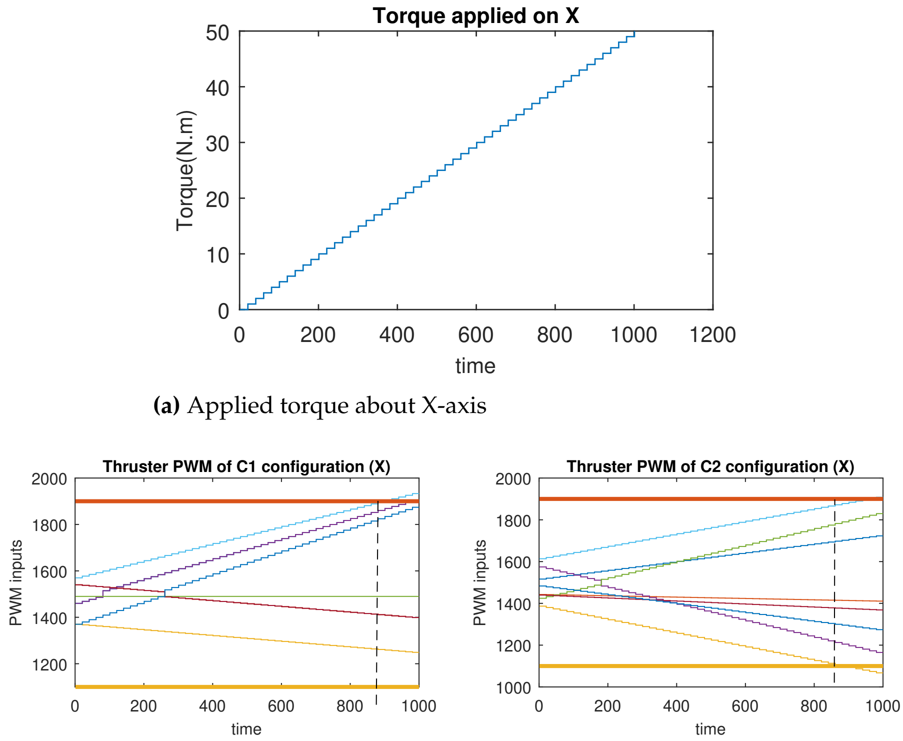

(a) Applied torque about X-axis

(b) PWM inputs of C1

(c) PWM inputs of C2

Figure 20. The simulation of cube rotation about X-axis for $\mathbf{C}^1$ and $\mathbf{C}^2$

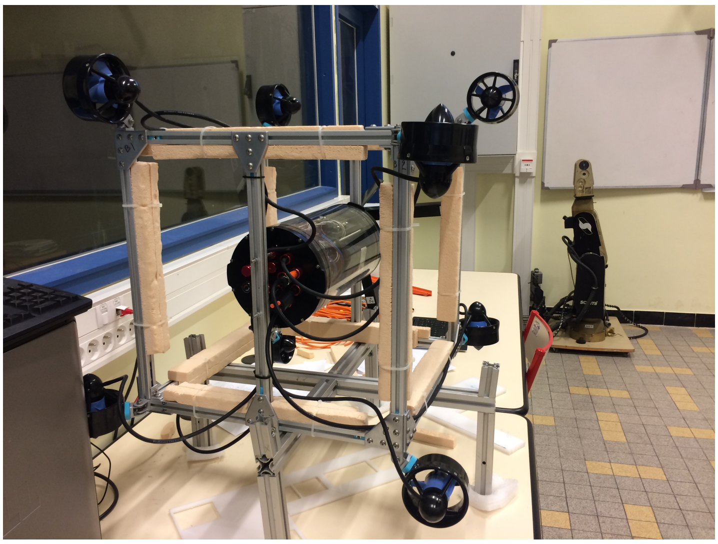

Figure 24. $\mathbf{C}^1$ configuration of Cube robot

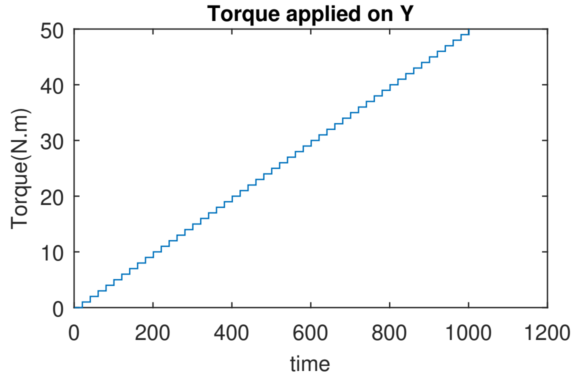

(a) Applied torque about Y-axis

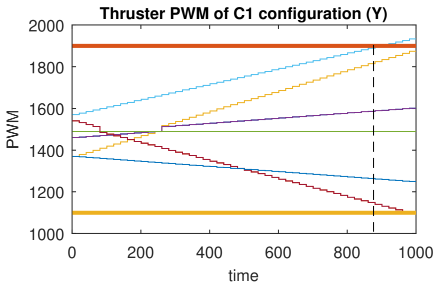

(b) PWM inputs of C1

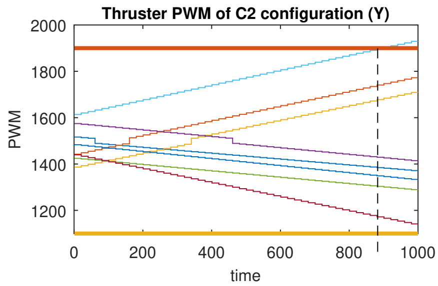

(c) PWM inputs of C2

Figure 21. The simulation of cube rotation about Y-axis for $\mathbf{C}^1$ and $\mathbf{C}^2$

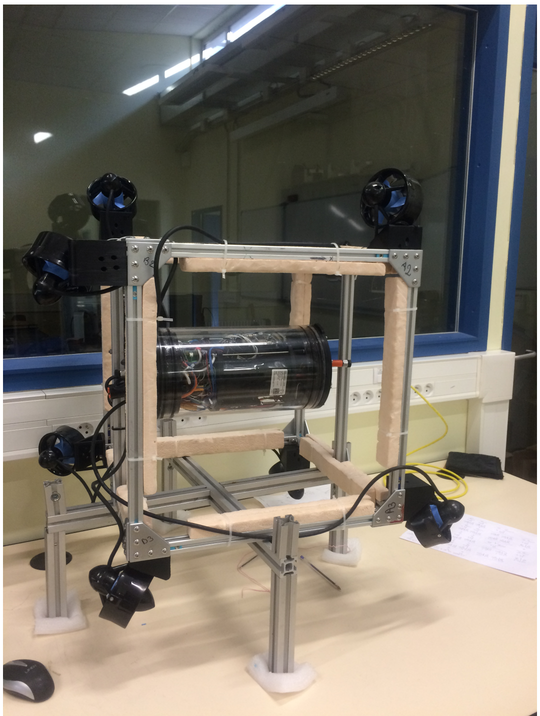

Figure 25. $\mathbf{C}^2$ configuration of Cube robot

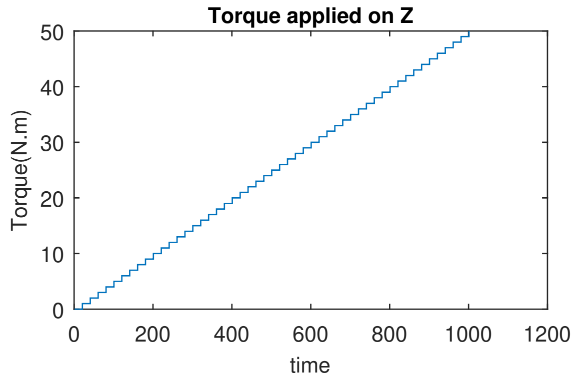

(a) Applied torque about Z-axis

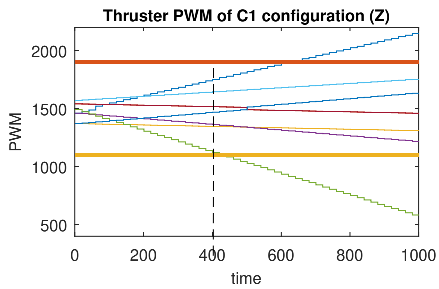

(b) PWM inputs of C1

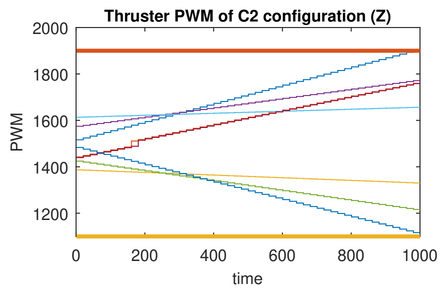

(c) PWM inputs of C2

Figure 22. The simulation of cube rotation about Z-axis for $\mathbf{C}^1$ and $\mathbf{C}^2$

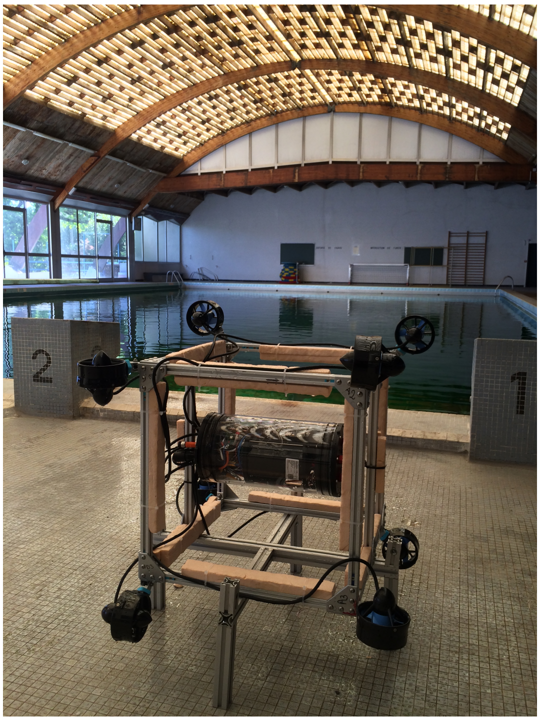

Figure 26. Swimming pool at Montpellier University

462 *6.1. Attainability validation*

463 An incremental torques about X-axis, Y-axis, and Z-axis are applied on cube robot
464 respectively, angular velocities and PWM input values are stored for evaluating these
465 two configurations. For safety, the experiments will be stopped when one thruster
466 reaches the saturation values. The experimental results are shown in Figures 27, 28 and

29. For rotating about X-axis, Figure 27, attainability of configurations $\mathbf{C}^1$ and $\mathbf{C}^2$ is almost the same, all thrusters operate in feasible region. Otherwise, for rotating about Y-axis and Z-axis, attainability of configuration $\mathbf{C}^2$ shows better $\mathbf{C}^1$ one. In particular, with Y-axis experiment (Figure 28), Cube robot with $\mathbf{C}^1$ stops the mission earlier than with $\mathbf{C}^2$ (at time step 771) because one thruster reach its saturation. The same thing happens with Z-axis experiment (at time step 451) (see Figure 29).

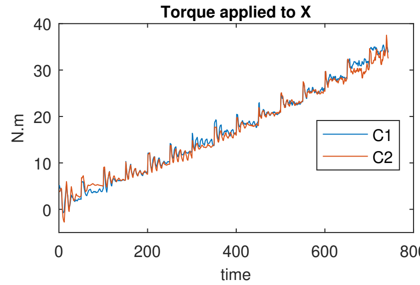

(a) Applied torque about X-axis

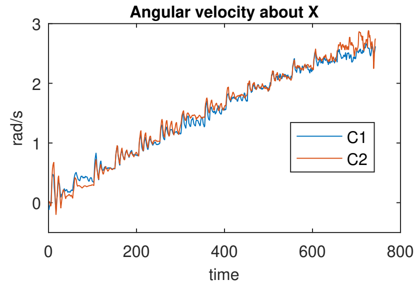

(b) Angular velocities

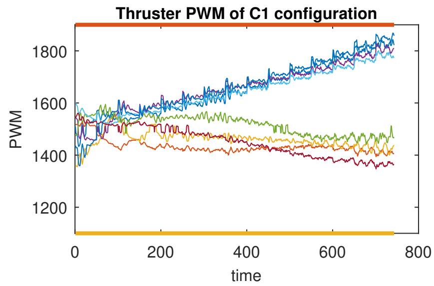

(c) PWM inputs of $\mathbf{C}^1$

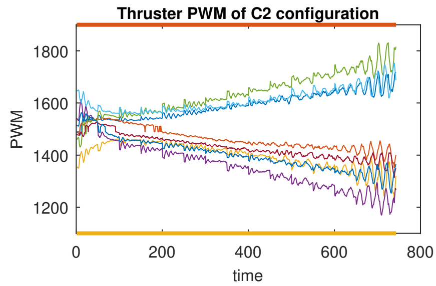

(d) PWM inputs of $\mathbf{C}^2$

Figure 27. The cube rotates about X-axis for $\mathbf{C}^1$ and $\mathbf{C}^2$

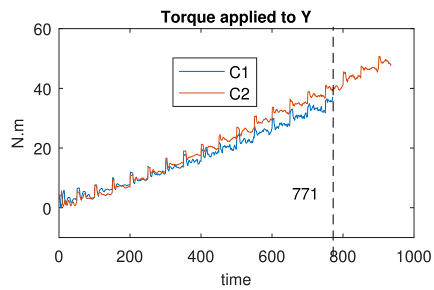

(a) Applied torque about Y-axis

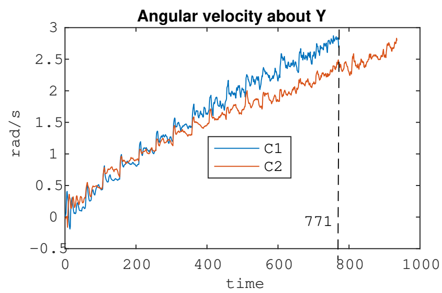

(b) Angular velocities

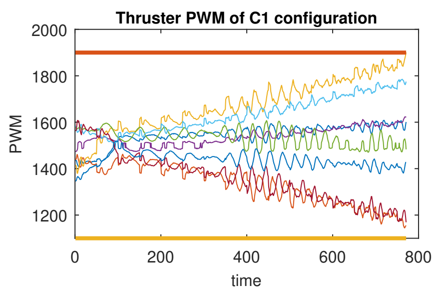

(c) PWM inputs of $\mathbf{C}^1$

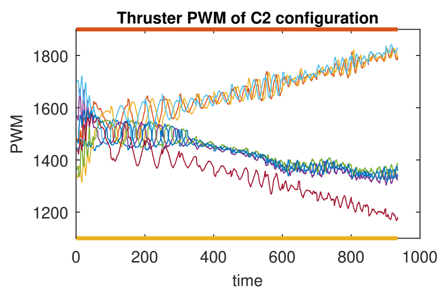

(d) PWM inputs of $\mathbf{C}^2$

Figure 28. The cube rotates about Y-axis for $\mathbf{C}^1$ and $\mathbf{C}^2$

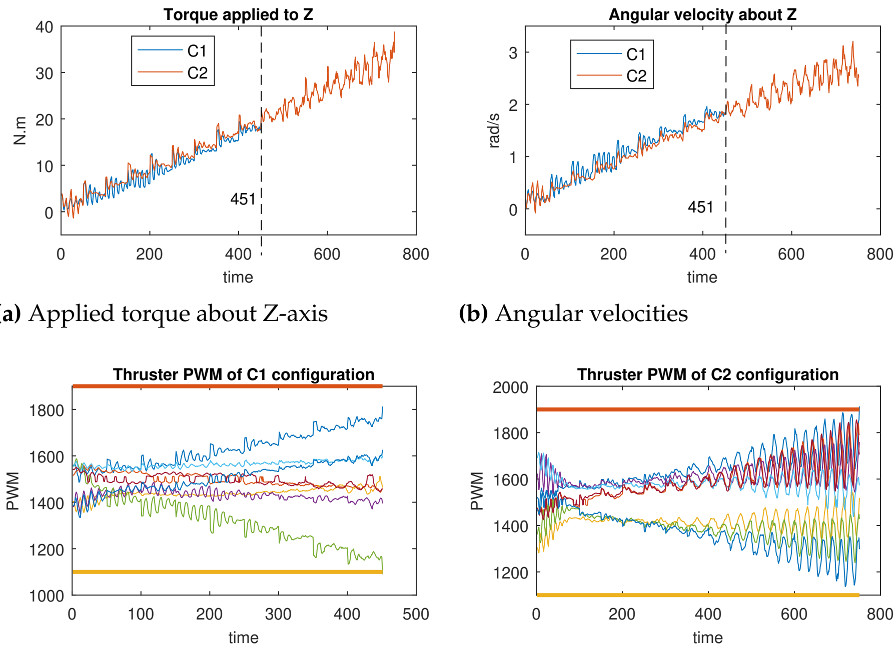

(a) Applied torque about Z-axis **(b)** Angular velocities

(c) PWM inputs of $\mathbf{C}^1$ **(d)** PWM inputs of $\mathbf{C}^2$

Figure 29. The cube rotates about Z-axis for $\mathbf{C}^1$ and $\mathbf{C}^2$

6.2. Energetic validation

In this section, we verify the energy ~~spending~~ during these experiments for two configurations. ~~For measuring, a~~n energy-like criterion is proposed:

$$\mathbf{E} = \sum_{i=1}^{m} \int_{t=0}^{T} |PWM^i(t) - 1500| dt \tag{43}$$

where m is the number of thrusters, T is the time of experiment, $PWM^i(t)$ is PWM inputs of i^{th} thruster.

Table 6 shows the energy consumption of robot during three rotations experiments. For X-axis rotation, the attainability of two configurations is the same but the the spent energy of $\mathbf{C}^2$ configuration is lower. For Y-axis and Z-axis rotation, the duration of experiments of $\mathbf{C}^2$ configuration is longer, the energy consumption, therefore, is higher.

Table 6. Energy consumption of two configurations

No.	Rotation	$\mathbf{E}_{\mathbf{C}^1}$	$\mathbf{E}_{\mathbf{C}^2}$
1	X	7.2303e+04	6.9603e+04
2	Y	7.5480e+04	1.0590e+05
3	Z	3.1637e+04	7.4350e+04

Table 7 shows the comparison of energy consumption of two configurations with the same time duration. For Y-axis rotation, the energy value of $\mathbf{C}^2$ configuration is lower than one of $\mathbf{C}^1$ configuration. However, for Z-axis, the energy value of $\mathbf{C}^2$ configuration is higher. This happens because the robot dived deeper for $\mathbf{C}^2$ configuration in experiment of Z-axis rotation, the robot had to deliver more power to keep at higher constant depth.

Table 7. Energy consumption of two configurations with the same time duration

No.	Rotation	$\mathbf{E}_{\mathbf{C}^1}$	$\mathbf{E}_{\mathbf{C}^2}$
1	Y	7.5480e+04	7.2715e+04
2	Z	3.1637e+04	3.3312e+04

6.3. Robustness and Reactive validation

This section validates the robustness and reactive of the optimal configuration ($\mathbf{C}^2$) in comparison with the normal one ($\mathbf{C}^1$). For robustness, the robot ~~does~~ a mission, and one or two thrusters ~~is~~ turned off. For the normal configuration $\mathbf{C}^1$, the mission will ~~be failed~~, and for the optimal configuration $\mathbf{C}^2$, the mission will be guaranteed. Specifically, for robustness index, we will carry out the following experiments:

1. The cube robot dives to predefined depth with all motors being in the normal operating conditions.
2. The cube robot dives to the same predefined depth with one vertical motor being stopped.
3. The cube robot dives to the same predefined depth with two vertical motors being stopped.
4. The cube robot dives to the same predefined depth with three motors being stopped (two vertical motors and one arbitrary motor)
5. The cube robot simultaneously dive to the same predefined depth and rotates about Z-axis with three motors being stopped (two vertical motors and one horizontal motor)

For reactive index, we measure how fast the robot changes missions. The following experiments are carried out:

1. The cube robot goes down at the predefined depth and goes up to another predefined depth and go down again at the former predefined depth.
2. In the sequel, the cube robot goes down at the predefined depth, rotates about X-axis, after that, rotates about Y-axis. The rotation time of each axis should be 60 second or longer.
3. ~~In the n~~ext, the cube robot goes down at the predefined depth, rotates about X-axis, after that, rotates about diagonal-axis (diagonal of the cube robot). The rotation time of each axis should be 60 second or longer.

The experimental results for robustness validation of $\mathbf{C}^1$ and $\mathbf{C}^2$ are shown in Figures 30, 31, and 32. In case of one or two motors stopped, the depth control performance of $\mathbf{C}^1$ and $\mathbf{C}^2$ are almost the same (see Figure 30). This holds because there also exits thrusters which are in charge of the mission. The differences is clear in case of three thrusters stopped (Figure 32), the performance of $\mathbf{C}^1$ is not guaranteed (Figure 31) and violations of PWM values ~~are happened~~ (see Figure 32a).

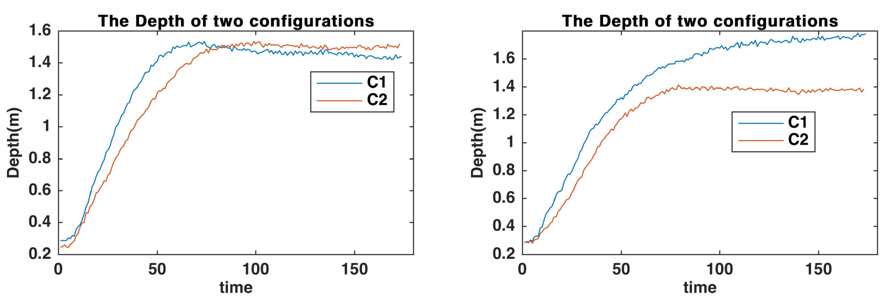

(a) Depth control of two configurations with one motor stopped

(b) Depth control of two configurations with two motor stopped

Figure 30. Depth control for $\mathbf{C}^1$ and $\mathbf{C}^2$ with one and two motors stopped

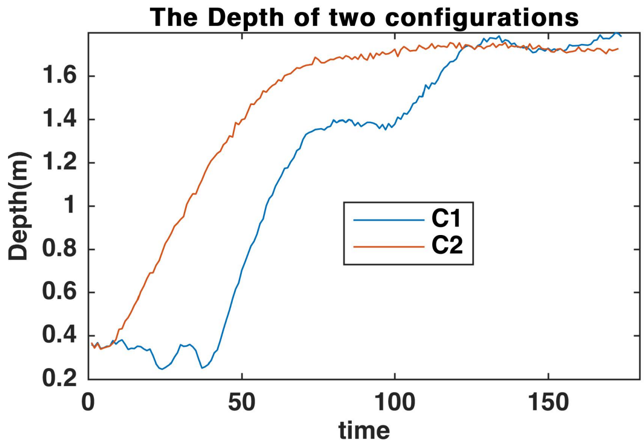

Figure 31. Depth control for $\mathbf{C}^1$ and $\mathbf{C}^2$ with three motors stopped

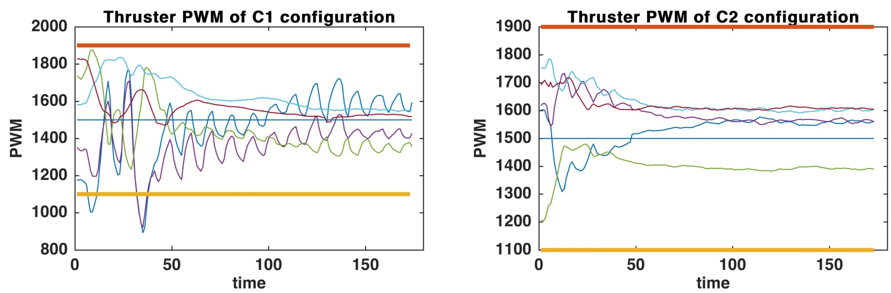

(a) PWM of $\mathbf{C}^1$ configuration **(b)** PWM of $\mathbf{C}^2$ configuration

Figure 32. PWM evaluation for $\mathbf{C}^1$ and $\mathbf{C}^2$ with 3 motors stopped

520 The results for reactive validation are shown in Figures 33, 34, and 35. We measure
521 the reactive time of angular velocities when changing the direction of Cube's actions.
522 It is clear that reactive time of $\mathbf{C}^2$ configuration is faster than one of $\mathbf{C}^1$ configuration.
523 Specifically, reactive time is the region formed by vertical dash lines in Figures 33, 34,
524 and 35. It is obvious to see that reactive time of $\mathbf{C}^2$ configuration is smaller than one of
525 $\mathbf{C}^2$ configuration (see Figure 34, and Figure 35).

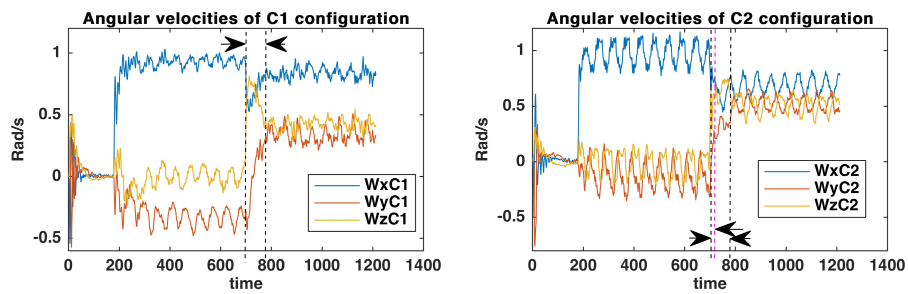

(a) Angular velocites of $\mathbf{C}^1$ configuration **(b)** Angular velocities of $\mathbf{C}^2$ configuration

Figure 33. Angular velocity evaluation for $\mathbf{C}^1$ and $\mathbf{C}^2$: diving, rotating X-axis, and rotating diagonal-axis

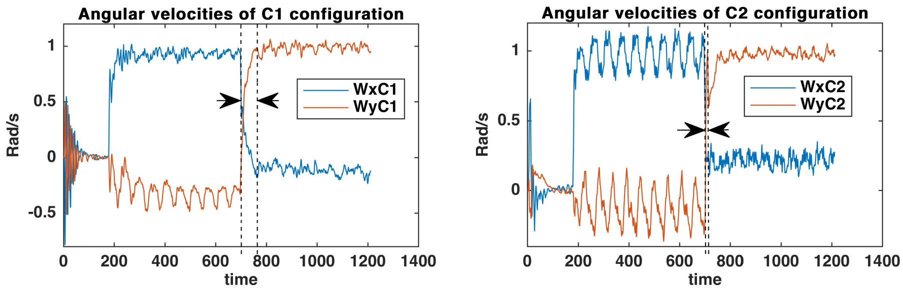

(a) Angular velocites of $\mathbf{C}^1$ configuration **(b)** Angular velocities of $\mathbf{C}^2$ configuration

Figure 34. Angular velocity evaluation for $\mathbf{C}^1$ and $\mathbf{C}^2$: diving, rotating X-axis, and rotating Y-axis

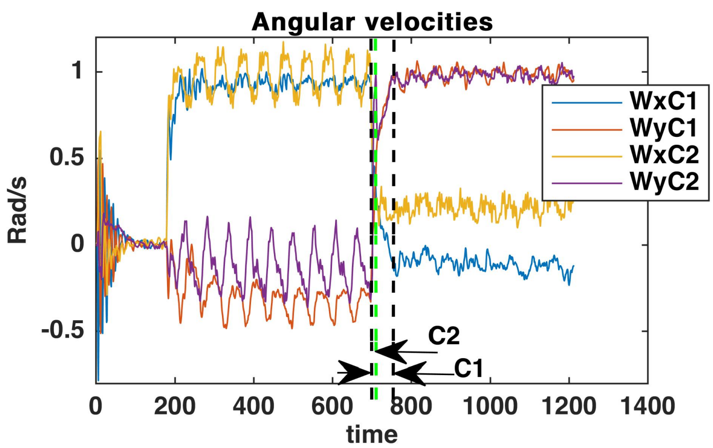

Figure 35. Angular velocity evaluation for $\mathbf{C}^1$ and $\mathbf{C}^2$: diving, rotating X-axis, and rotating Y-axis

7. Conclusion and future work

In this paper a procedure for designing configuration matrix (positions and directions of actuators) of over-actuated underwater robots is presented. The performance indices are proposed and analyzed. Multi-objective optimization problem is ~~formed~~ and solved. One Pareto optimal solution is found by goal attainment method. Simulation and experimental results show that its performances are better than a normal configuration which is often used in designing actuators. Finding all Pareto optimal solutions, Pareto front, remains a challenging problem and will be a future work. Moreover, a design problem relaxing the assumptions is also an interesting direction for future researches.

Author Contributions: Conceptualization, T.Dang, L.Lapierre, and R.Zapata.; methodology, T.Dang, L.Lapierre, and R.Zapata.; software, T.Dang., B.Ropars., P.Lepinay.; validation, T.Dang, L.Lapierre, R.Zapata., B.Ropars, P.Lepinay.; writing—original draft preparation, T.Dang.; writing—review and editing, L.Lapierre.; supervision, L.Lapierre., R.Zapata.; project administration, L.Lapierre.; funding acquisition, L.Lapierre. All authors have read and agreed to the published version of the manuscript.

Acknowledgments: The authors would like to thank Numev Labex, MUSE, Montpellier University; Region Occitanie; and FEDER for supporting this research.

Conflicts of Interest: The authors declare no conflict of interest.

Appendix A Appendix

Theorem A1. *The image of the unit hyper-sphere under any $n \times m$ matrix is a hyper-ellipsoid.*

Proof. Let $\mathbf{A}$ be a $n \times m$ matrix with rank r. Let $\mathbf{A} = \mathbf{USV}^T$ be a singular value decomposition of $\mathbf{A}$. The left and right singular vectors of $\mathbf{A}$ are denoted as $\mathbf{u}_1, \mathbf{u}_2, ..., \mathbf{u}_n$

and $\mathbf{v}_1, \mathbf{v}_2, ..., \mathbf{v}_m$, respectively. Since $rank(A) = r$, the singular values of $\mathbf{A}$ have the properties: $\sigma_1 \geq \sigma_2 \geq ... \geq \sigma_r > 0$ and $\sigma_{r+1} = \sigma_{r+2} = ... = \sigma_m = 0$.

Let $\mathbf{x} = \begin{pmatrix} x_1 \\ \vdots \\ x_m \end{pmatrix}$ be an unit vector in $\mathbb{R}^m$. Because $\mathbf{V}$ is an orthogonal matrix, and $\mathbf{V}^T$ is also, we have $\mathbf{V}^T\mathbf{x}$ is an unit vector (it is easy to see that $\|\mathbf{V}^T\mathbf{x}\| = \|\mathbf{x}\|$). So, $(\mathbf{v}_1^T\mathbf{x})^2 + (\mathbf{v}_2^T\mathbf{x})^2 + ... + (\mathbf{v}_m^T\mathbf{x})^2 = 1$.

On the other hand, we have $\mathbf{A} = \sigma_1\mathbf{u}_1\mathbf{v}_1^T + \sigma_2\mathbf{u}_2\mathbf{v}_2^T + ... + \sigma_r\mathbf{u}_r\mathbf{v}_r^T$. Therefore:

$$\begin{aligned} \mathbf{Ax} &= \sigma_1\mathbf{u}_1\mathbf{v}_1^T\mathbf{x} + \sigma_2\mathbf{u}_2\mathbf{v}_2^T\mathbf{x} + ... + \sigma_r\mathbf{u}_r\mathbf{v}_r^T\mathbf{x} \\ &= (\sigma_1\mathbf{v}_1^T\mathbf{x})\mathbf{u}_1 + (\sigma_2\mathbf{v}_2^T\mathbf{x})\mathbf{u}_2 + ... + (\sigma_r\mathbf{v}_r^T\mathbf{x})\mathbf{u}_r \\ &= \mathbf{y}_1\mathbf{u}_1 + \mathbf{y}_2\mathbf{u}_2 + ... + \mathbf{y}_r\mathbf{u}_r \\ &= \mathbf{Uy} \end{aligned} \tag{A1}$$

where $\mathbf{y}_i$ denotes the $\sigma_i\mathbf{v}_i^T\mathbf{x}$, and $\mathbf{y} = \begin{pmatrix} y_1 \\ \vdots \\ y_r \end{pmatrix}$.

From (A1), we have: $\|\mathbf{Ax}\| = \|\mathbf{Uy}\| = \|\mathbf{y}\|$ (since $\mathbf{U}$ is an orthogonal matrix). Moreover, $\mathbf{y}$ has the following property:

$$\begin{aligned} &(\frac{y_1}{\sigma_1})^2 + (\frac{y_2}{\sigma_2})^2 + ... + (\frac{y_r}{\sigma_r})^2 = \\ &= (\mathbf{v}_1^T\mathbf{x})^2 + (\mathbf{v}_2^T\mathbf{x})^2 + ... + (\mathbf{v}_r^T\mathbf{x})^2 \leq 1 \end{aligned} \tag{A2}$$

Specifically:

1. If $r = m$ (of course, we must have $m \leq n$), the equality in Equation (A2) holds, and the image of unit hyper-sphere forms the surface of a hyper-ellipsoid.
2. If $r < m$, the image of unit hyper-sphere corresponds to a solid hyper-ellipsoid.

This completes the proof. □

References

1. Lapierre, L. Robust diving control of an AUV. *Ocean Engineering* **2009**, *36*, 92–104.
2. Lapierre, L.; Jouvencel, B. Robust nonlinear path-following control of an AUV. *IEEE Journal of Oceanic Engineering* **2008**, *33*, 89–102.
3. Levine, W.S. *The Control Systems Handbook: Control System Applications*; CRC press, 2010.
4. Johansen, T.A.; Fossen, T.I. Control allocation—A survey. *Automatica* **2013**, *49*, 1087 – 1103.
5. Ropars, B.; Lapierre, L.; Lasbouygues, A.; Andreu, D.; Zapata, R. Redundant actuation system of an underwater vehicle. *Ocean Engineering* **2018**, *151*, 276 – 289. doi:https://doi.org/10.1016/j.oceaneng.2017.12.025.
6. Nakamura, Y.; Hanafusa, H.; Yoshikawa, T. Task-priority based redundancy control of robot manipulators. *The International Journal of Robotics Research* **1987**, *6*, 3–15.
7. Adorno, B.V.; Fraisse, P.; Druon, S. Dual position control strategies using the cooperative dual task-space framework. IROS'10: International Conference on Intelligent Robots and Systems. IEEE, 2010, pp. 3955–3960.
8. Agravante, D.J.; Sherikov, A.; Wieber, P.B.; Cherubini, A.; Kheddar, A. Walking pattern generators designed for physical collaboration. Robotics and Automation (ICRA), 2016 IEEE International Conference on. IEEE, 2016, pp. 1573–1578.
9. Pham, T.H.; Caron, S.; Kheddar, A. Multicontact Interaction Force Sensing From Whole-Body Motion Capture. *IEEE Transactions on Industrial Informatics* **2018**, *14*, 2343–2352.
10. Yoshikawa, T. Dynamic manipulability of robot manipulators. Proceedings. 1985 IEEE International Conference on Robotics and Automation, 1985, Vol. 2, pp. 1033–1038. doi:10.1109/ROBOT.1985.1087277.
11. Yoshikawa, T. *Foundations of robotics: analysis and control*; Mit Press, 1990.
12. Kumar, A.; Waldron, K. The workspaces of a mechanical manipulator. *Journal of Mechanical Design* **1981**, *103*, 665–672.
13. Paden, B.; Sastry, S. Optimal kinematic design of 6R manipulators. *The International Journal of Robotics Research* **1988**, *7*, 43–61.
14. Park, F.C.; Brockett, R.W. Kinematic dexterity of robotic mechanisms. *The International Journal of Robotics Research* **1994**, *13*, 1–15.
15. Pierrot, F.; Benoit, M.; Dauchez, P. Optimal thruster configuration for omni-directional underwater vehicles. SamoS: a Pythagorean solution. OCEANS '98 Conference Proceedings, 1998, Vol. 2, pp. 655–659 vol.2. doi:10.1109/OCEANS.1998.724320.
16. Kharrat, H. Optimization of Thruster Configuration for Swimming Robots. Master's thesis, Rice University, 2015.

17. Stephan, J.; Fichter, W. Fast Exact Redistributed Pseudoinverse Method for Linear Actuation Systems. *IEEE Transactions on Control Systems Technology* **2017**, *PP*, 1–8. doi:10.1109/TCST.2017.2765622.
18. Grechi, S.; Caiti, A. Comparison between Optimal Control Allocation with Mixed Quadratic & Linear Programming Techniques. *IFAC-PapersOnLine* **2016**, *49*, 147 – 152. 10th IFAC Conference on Control Applications in Marine SystemsCAMS 2016, doi:https://doi.org/10.1016/j.ifacol.2016.10.335.
19. Ropars, B.; Lasbouygues, A.; Lapierre, L.; Andreu, D. Thruster's dead-zones compensation for the actuation system of an underwater vehicle. Control Conference (ECC), 2015 European. IEEE, 2015, pp. 741–746.
20. Yoshikawa, T. Manipulability of robotic mechanisms. *The international journal of Robotics Research* **1985**, *4*, 3–9.
21. Olver, F.W.; Lozier, D.W.; Boisvert, R.F.; Clark, C.W. *NIST handbook of mathematical functions hardback and CD-ROM*; Cambridge university press, 2010.
22. Trefethen, L.N.; Bau III, D. *Numerical linear algebra*; Vol. 50, Siam, 1997.
23. Gembicki, F.; Haimes, Y. Approach to performance and sensitivity multiobjective optimization: The goal attainment method. *IEEE Transactions on Automatic control* **1975**, *20*, 769–771.
24. BlueRobotics. BlueRobotics. https://bluerobotics.com/.